CRISTINA ARIZA-CARRICONDO (Orcid ID: 0000-0003-3987-9481)

Two types of installation of 3D-printed Zero Tension Lysimeter for soil leaching and Water Bucket Model validation

Running title: 3D-printed lysimeters and WBM for soil leaching

CRISTINA ARIZA-CARRICONDO[a], ERIC STRUYF[a], MARILYN ROLAND[a] , BERT GIELEN[a], CAROLINE VINCKE[b] AND IVAN A. JANSSENS[a]

[a] *University of Antwerp, Department of Biology, Research group Plants and Ecosystems (PLECO), Universiteitsplein 1, Wilrijk, Belgium*

[b] *Earth and Life Institute, Université Catholique de Louvain, Croix du Sud 2 ,Louvain-la-Neuve, Belgium*

Correspondence : Cristina Ariza-Carricondo, E-mail: cristina.arizacarricondo@uantwerpen.be

Keywords: Soil drainage, sampler design, flux validation, water balance, dissolved compounds tracing

This article has been accepted for publication and undergone full peer review but has not been through the copyediting, typesetting, pagination and proofreading process which may lead to differences between this version and the Version of Record. Please cite this article as doi: 10.1111/ejss.13295

Abstract

Quantifying and analyzing leaching water is essential to understand water and nutrient cycles and the vertical transport of elements through soils. Zero Tension Lysimeters (ZTLs) have been widely used to capture the soil solution leaching by gravity. This study designed and evaluated a 3D-printed ZTL (ZTL^{3D}) with specific characteristics and materials to quantitatively capture dissolved element fluxes. By 3D-printing the ZTLs, we were able to include specific 3D structures and precise details in the design allowing samplers installation from the surface rather than trenches, and thus avoiding the need for installation trenches to remain open. The ZTLs^{3D} connect directly with the surface, do not depend on secondary collectors, can be installed at any depth and samplers are easily retractable when dismantling the field set up. The material used, Nylon 12, was tested for DOC release. The ZTL^{3D} design was printed in two different external shapes while characteristics and internal design were identical. The difference in external shape was to study the effects of two contrasting types of installation: a cylindrical sampler for vertical installation (by soil coring from the surface) and a rectangular samplers for horizontal installation (from a pit or a trench wall). We installed them at different depths (2, 30 and 75 cm) in a forest soil and conducted rainfall simulation experiments. A Water Bucket Model (WBM), created to calculate the water drainage fluxes that the ZTLs^{3D} should collect, reproduced very well the variation in soil water content measured by soil moisture sensors installed adjacent to the ZTLs^{3D} at 16, 30, 50 and 75 cm depth. Drainage fluxes simulated by the WBM showed that the vertical installation performed better at collecting water at all depths than the horizontally installation, but overall the ZTLs^{3D} failed to collect the simulated amounts of drainage water. Nonetheless, the ZTLs^{3D} did collect leachate water, enabling their chemical analysis. Combining the concentrations in the water

collected by the $ZTLs^{3D}$ with the modeled drainage fluxes does allow estimation of DOC- and elemental leaching rates. This article presents the novel design of these two types of $ZTLs^{3D}$ because future improvements may result in better performance, and discusses their (dis)agreement with the modelled WBM fluxes.

1. Introduction

Lysimeters are devices that collect soil water, allowing to determine the chemical composition of the leaching water. In the past decades, lysimeters have contributed substantially to advances in soil science (Abdulkareem *et al.*, 2015; Singh *et al.*, 2018; Dabrowska & Rykala, 2021) and agricultural research. As a result, numerous lysimeter types and applications have been proposed, ranging from very basic water collectors to sophisticated weighing devices that allow estimating water drainage fluxes (Meissner et al., 2020).

Zero Tension Lysimeters (ZTLs) have been built from variable materials, with sizes adapted to specific research needs. They are less commercialized than Tension Lysimeters (TLs) or Weighable Lysimeters (WL), and a variety of project-specific applications have been put forward. Mostly, ZTLs are inserted horizontally from the wall of a pit or trench into the soil. They are linked to a lower placed bottle that acts as a collector at the bottom of the trench. ZTLs collect water only when the soil immediately above them has positive water pressure as no tension is applied. However, water has been reported to flow from ZTLs into the surrounding soil when the latter dries due to the difference in pressure between the inside and outside of the sampler, resulting in potential underestimation of soil water flow volume (Kosugi & Katsuyama, 2004). In addition, the installation of ZTLs is often destructive, leading to physical disturbance of the soil column (Mohamed, 2012; Abdulkareem *et al.*, 2015). Although ZTLs mainly collect rapid drainage water, such as preferential flows (Legout *et al.*, 2009), they tend to represent a more natural indication of water flow and concentrations of solutes than TLs, as no tension is applied (Makowski *et al.*, 2020).

For collecting leaching water without tension, the soil water content needs to exceed Field Capacity (FC), defined as "the amount of water held in the soil after the excess gravitational water has drained away and after the rate of downward movement of water has materially decreased" (Veihmeyer & Hendrickson, 1931). When FC is exceeded, water descends to deeper layers by gravity, allowing it to be captured by the ZTL. The question remains whether the amount of collected water is representative for the true drainage flux.

When quantification of drainage water is the goal, the distortion made by the installation creates uncertainties, and preferential flow pathways (PFP) may confound the measurements. Preferential flow pathways (PFP) are any macropores, fingers, funnels and hydrophobicity-induced flow paths that make water move rapidly, carrying dissolved and/or suspended matter through the profile and affecting nutrient transport and related fluxes (Makowski *et al.*, 2020). Vogel et al. (2000) mentioned that textural differences rather than structural effects, form some preferential flow pathways. These types, called fingering and funnel flow, are created by gravity-driven flow and water-repelling soil when texture changes from fine to coarse. Preferential flow pathways are common in unsaturated soils, and high flow rates often occur during high-intensity rainfall events (Stumpp & Maloszewski, 2010), influencing infiltration and recharge contaminant transport and ecohydrology (Nimmo, 2012). Preferential flow pathways severely limit water and solute movement prediction in structured or macroporous soils (Vogel *et al.*, 2000).

Here, we present a novel design of 3D-printed ZTLs (ZTLs^{3D}) with two different external shapes adapted to specific types of installation. The different shapes were made to facilitate connection between the ZTLs^{3D} and the surrounding soils and compare the impact of the disturbance caused by the two different types of installations in the field. Our main objective is to simultaneously quantify the volume of leaching water and collect this water for analysis of trace solutes through the soil depth profile during natural rain events and during heavy rainfall simulation experiments. The ZTLs^{3D} were installed at 2 cm below the litter layer and at 30 and 75 cm depth in the soil. We tested two types of installation, vertical and horizontal, each corresponding to a specific external shape of the design (see below for details). Earlier studies primarily compared different types of lysimeters, for instance, tension versus non-tension lysimeters, or compared lysimeters to other techniques (Cabrera Corral *et al.*, 2016; Farsad *et al.*, 2019) The novelty of this research lies in comparing two types of installation of the same ZTL^{3D} (same internal design, different external shapes), studying the effect of the installation type on the performance of the samplers using a Water Bucket Model (WBM) as validation.

2. Design and methodology

2.1 Site description

The experimental site is located in the forest 'De Inslag' in Brasschaat near Antwerp, Belgium (51°18'27.1"N 4°31'18.9"E). The experiment is hosted in the vicinity of the ICOS ecosystem monitoring station of Brasschaat (Franz *et al.*, 2018; Heiskanen *et al.*, 2021; www.icos-ri.be), co-located with an ICP forest intensive monitoring level II plot (Neirynck *et al.*, 2008). The location of this research is mainly covered by an even-aged Scots pine plantation (Pinus sylvestris L., planted in 1929), while the larger area can be characterized as a mixed coniferous/deciduous forest. The mean annual temperature at the site is 10.8 °C, with a mean annual precipitation of 1011 mm, with drier periods for the years 2004 (897 mm), 2011 (888 mm), 2013 (867 mm) (Horemans *et al.*, 2020) and 2019 (798 mm). The herb layer of the Scots pine stand is dominated by Molinia caerulea (L.) Moench, followed by saplings of Sorbus aucuparia L., Rubus species and Dryopteris ferns (Gielen *et al.*, 2011). The site is characterized by moderately wet sandy soil, rarely saturated, high hydraulic conductivity in the upper layers and distinct humus and/or iron B horizon. The soil is classified as Endogleyic Brunic, Albic Hypoluvic, Arenosol (Dystric) according to IUSS Working Group (IUSS Working Group WRB, 2007) with a C:N ratio of 30 in the organic layer. Clay lenses of variable thickness locally hamper the infiltration of water at 50–125 cm depth, and pH values of the soil water range from 3.1-3.9 (Janssens *et al.*, 1999; Verstraeten, 2018).

2.2 Laser printing and material

We here present a new design of ZTL, fit for 3D printing. The ZTL^{3D} was created by Selective Laser Sintering (SLS) (Beaman & Deckard, 1990), a process that uses powder material (Nylon 12) and a laser beam, allowing to achieve extreme accuracy in small details in the design.

Printing was done on a Multi Jet Fusion 3D printer HP, a powder bed additive manufacturing technique. In SLS, the process can be resumed in three steps: First, the printer deposits a layer of powder. Secondly, the printhead sprays a fusing and detailing agent on the powder. As a final step, a strong lamp fuses the powder only where the fusing agent was sprayed, and then the process starts again for the next layer (Kim *et al.*, 2016). The powder used has two purposes, acting both as the holder during the printing process *(*Zhu *et al.*, 2015) and as the material chosen, as the powder is fused to form the structure desired. Once the fusing process is finished, the remaining powder is blown out from the inside of the sampler, process called "sand blasting", and subsequently repeatedly flushed out with water. The minimum layer thickness is 0.08 mm.

The material chosen to SLS print was the high molecular weight Polyamide 12 or Nylon 12, which is characterized by low moisture absorption (~2%), exceptional impact and notched impact strength, resistance to extreme temperatures, resistance against greases, oils, fuels, hydraulic fluids, various solvents, salt solutions and other chemicals (more properties in McKeen, 2017). To test the influence of Nylon12 on DOC and nutrient concentrations, we ran a sensitivity analysis to test their release from the $ZTLs^{3D}$. Distilled water was held in several $ZTLs^{3D}$. Part of them did not receive any cleaning treatment after printing, the other part were pre-washed in an ultrasonic bath for 60 min at 60 ^{o}C in two intervals of 30 min. Concentrations were analyzed after one day, three days, six days and 30 days to afterwards refill the $ZTLs^{3D}$ with new distilled water and measured their concentrations once again after 15 days.

2.3 Specific design

We designed two models of the ZTLs^{3D}. One is formed by one single cylindrical volume of 13 cm height and 8 cm diameter and has a water collection capacity of ~350 ml. The second one is a square prism of 13 cm height and 8.5 cm width, with a capacity of ~450 ml.

The cylindrical ZTLs^{3D} (Fig. 1) fit in a cylindrical hole made by soil coring from the soil's surface, hereafter referred to as vertical installation. The square ZTLs^{3D} (Fig. 2) are fit for installation in a cubic hole made in a trench wall, hereafter referred to as horizontal installation.

To avoid soil particles, plant litter, or soil animals from falling into the ZTLs^{3D}, in both designs, the ZTLs^{3D} have two meshes at 7 cm from the sampler's bottom: one of the meshes is SLS-printed (Fig. 1e and Fig. 2e), with a pore width of 1 mm. Its purpose is to give support to the other mesh, which is made from aluminium and has an 80 µm pore diameter. To hold the aluminium mesh in place, an SLS-printed ring keeps the two meshes together (Fig. 1 and Fig. 2f). This system was designed to avoid the use of glue or any other chemical to avoid DOC pollution of the collected water samples.

By having the two meshes and a ring in the middle of the sampler, we created two compartments, even though this is a one-piece sampler (Fig. 1 and Fig. 2b). On top of the meshes, the upper compartment was filled with 2-3 cm of high water-conductive sand, facilitating the water on top of the sampler to flow inside (Makowski *et al.*, 2020.; Singh *et al.*, 2018). Above this layer of high water-conductive sand, there is a 2-3 cm soil layer with autochthonous soil from the corresponding soil horizon where the ZTLs^{3D} are installed.

The bottom part, where the leached water is collected, has a 10° sloping bottom that drives the collected water towards the bottom exit (Fig. 1a and Fig. 2a). The cylindrical design has four rings printed outside the structure (Fig. 1c). These rings can be equipped with ropes during installation to facilitate extraction of the sampler from deep installations at the end of the study.

Polytetrafluoroethylene (PFTE) tubes that lead to the surface are connected to the two exits at the bottom of the sampler. The exits are printed in a specific shape to allow a stable connection between the sampler and the tubing used to extract the water to the surface. The bottom exit is used for water extraction, while the upper exit enables air to enter when water is collected, thus avoiding under-pressure in the ZTLs^{3D} and facilitating the extraction of all water collected in the ZTLs^{3D}. To limit the amount of residue water that cannot be collected, the bottom exit was placed as low as possible, and its inner diameter was minimized to 2 mm. The water extraction is accomplished by connecting a pump to the PFTE tubing connected to the bottom exit of the ZTLs^{3D}. Specific sampler characteristics, such as the angled bottom slope and the double exit for air and water circulation are based on Thompson *et al.'s* (1995) design. Water is sucked up to the surface and collected in a recipient (dark glass bottle for DOC) for further analyses. There is thus no need to keep trenches or pits open after installation of the ZTL^{3D} in order to sample.

Costs of ZTLs can vary greatly; the most affordable method is self-fabrication, with estimations of material cost from 20 – 60 € per sampler (Mohamed, 2012, Thompson *et al.*, 1995). Commercially available ZTLs are scarce and range around 300 € (https://www.soilmoisture.com/zero-tension-lysimeter-pvc-tube-for-45-degree-insertion/). In our case, a single ZTLs^{3D} has a printing cost of ~80 €. The cost of the aluminium mesh, together with the PFTE tubing, add a few extra € per ZTL^{3D}. Depending on the installation depth, the cost will thus vary slightly due to the different lengths of the PFTE tubes. The quality of the ZTLs^{3D} can be compared with the characteristics found in commercialized samplers thanks to the highly accurate 3D-laser printing process, which is ideal for achieving small details, while the total cost can be compared to self-made samplers.

The printing process for both ZTLs^{3D} designs lasted around 50 hours to produce 20 ZTLs^{3D}. During the first 24 hours, the samplers are 3D laser printed, followed by another 24 hours of cooling down and another two hours of sandblasting as the finishing step.

The 3D designs are available in the following link; https://icos-belgium.be/files/Ariza-CarricondoCetAl.-DesignsZTLs.zip

2.4 Installation

The square ZTL^{3D} (Fig. 2) was designed to collect leachate water from an undisturbed soil column above the sampler (Fig. 3 and 4). However, this complicates the installation: trenches are needed to allow horizontal installation at specific depths, which causes disturbance to the surrounding forest soil. Although the square ZTL^{3D} could be installed in any soil whenever a trench is made, here we tested their performance in large soil monoliths. We made 1.3 m deep trenches to create 16 soil monoliths of 2 m x 2 m , grouped in four monoliths per plot (Fig. 3).

In every monolith, four ZTLs^{3D} were installed at three depths. First, a 25 cm deep rectangular hole was dug horizontally in the trench wall, wherein two square ZTLs^{3D} were inserted at each depth (2 cm in the soil surface under the litter layer and 30 cm and 75 cm below the soil surface) and subsequently pushed up into the soil column above and underfilled to maintain direct contact between the sampler and the soil. In total, 96 square ZTLs^{3D} were installed in the 16 monoliths. After this type of installation, monoliths were individually isolated, wrapped (except the surface) with two foils, the first one a strong plastic foil that acts as a barrier to prevent the water from leaving or entering, the second foil being a cloth that protects the monoliths from roots growing in (Fig. 3). Once this step was finished, the trenches were refilled.

In the same monoliths, two cylindrical ZTLs^{3D} (Fig. 1 and 4) were installed vertically at each depth: 2 cm under the littler layer and at 30 cm and 75 cm from the surface. Note that the soil core depths reported here were counted from the upper part of the sampler to the surface: the actual depth of the soil core was thus 13 cm deeper (height of the ZTLs^{3D}). Figure 4 shows, in red, the areas of soil affected by the installation. Again, trenches are not required for the vertical installation, but instead, the disturbance comes from soil coring; therefore, the vertically installed ZTLs^{3D} collect water from a disturbed soil column.

In addition to the 96 square ZTLs^{3D}, a total of 96 cylindrical ZTLs^{3D} were installed in the 16 monoliths. In summary, 12 ZTLs^{3D} per monolith were installed, each at least 50 cm apart, two replicates per depth and per type of installation (vertical or horizontal), creating a total of 64 samplers per depth. Furthermore, apart from the ZTLs^{3D}, every monolith was equipped with four TDRs, at 16 cm, 30 cm, 50 cm and 75 cm (CS605-L-3-Rod TDR Probe with RG58 Cable, Campbell Scientific, Logan, USA) and five handmade pluviometers were randomly positioned around every group of four monoliths.

Several measures were taken to minimize the disturbance created by vertical installation. Before soil coring, the litter layer was carefully removed and kept apart. At the end of the installation, it was placed back on the surface as intact as possible. Every extracted soil core was kept separate, and the soil columns were carefully reconstructed after ZTLs^{3D} installation by placing the extracted soil cores at their original depth. Nonetheless, impact on soil structure, and thus water flow is unavoidable in case of vertical installation but to minimize the creation of preferential flow pathways directly above the ZTLs^{3D}, extracted soil cores were

2.5 times wider than the $ZTLs^{3D}$ (20 cm compared to 8 cm) and the soil cores were reconstructed with the aim of reproducing the same bulk density as before (ensured by adding the same volume of extracted soil to the same volume of free space in the core).

2.5 Irrigation setup

Water collection started in February 2019. Natural rain events were intended to be collected biweekly, but this was not feasible due to the severe drought in spring 2019. Consequently, sampling was done after every 'collectable' rain event, meaning every rain event that brought the soil water content above FC, and thus potentially caused water drainage and element leaching. After that, more frequent water collection was made possible by the installation of an irrigation system. It consisted of 100 irrigation lines per monolith of 4 m^2, positioned every 20 cm for homogenous soil irrigation. Lines were directly installed on the surface of the soil. Water input was regulated by the irrigation system's valves with a velocity of 10 L min^{-1}. Sixteen flowmeters traced the amount of water added to every single monolith. From July 2019 onwards, this irrigation system was used to simulate rain events of different intensities. These rainfall simulation experiments were conducted in July, August, September, November 2019 and March 2020. The rain simulations applied had different objectives: 1. To allow a more frequent collection of element leaching by the $ZTLs^{3D}$, 2. The evaluation of the two types of $ZTLs^{3D}$ soil installations, 3. The study of element leaching under future climate conditions. 4. The trace of element leaching through depth in all climate scenarios. To achieve these goals, we simulated different rain intensities by adding 9-75 mm of irrigation water.

2.6 Water Bucket Model

We validated the water collection by the $ZTLs^{3D}$ using a Water Bucket Model (WBM), driven by water inputs via irrigation and precipitation (Pr), and water losses via evapotranspiration

(ET) and infiltration rate (IR). This model calculated the water content at the depths of the TDRs, whose measurements were used to validate the model. The WBM calculated the leaching water that every ZTL^{3D} should have collected following every rain or irrigation event, and then the modelled collections were used to test the performance of the $ZTLs^{3D}$.

Total water inputs were set as the sums of irrigation water plus the throughfall collected by 20 pluviometers installed around our soil monoliths. Because the throughfall collectors provided total water inputs for certain periods, and not the continuous data required by the WBM, we used the temporal variation in half-hourly precipitation data provide by the ICOS station to distribute the total collected by the pluviometers over the entire collection period. On average, we observed that 45% of the precipitation, measured on top of the flux tower less than 100 m away from our experimental site, reached the forest floor as throughfall. Evapotranspiration was more challenging to estimate because our monoliths excluded tree roots, implying that only soil evaporation and transpiration by ground vegetation occurred, not transpiration by the trees. As such, we could not use the evapotranspiration measured on the flux tower in our WBM. To this end, we split the year into four seasons, determined by the phenology of the ground vegetation, and for each period, reduced the measured evapotranspiration rates measured by the ICOS flux tower by a different factor. This factor was optimized to achieve a maximal fit between the WBM outputs and the TDR measurements.

Because the 16 monoliths were distributed over four different irrigation regimes, separate simulations with the WBM were performed using the specific water additions per treatment.

The WBM included the following formulas:

If (i) = the actual time step, (i -1) = previous time step and (layer) = refers to the chosen soil layer for applying the WBM (Litter layer or 2 cm, 30 cm and 75 cm depth).

1. Gross Input$_{layer\ i}$ (Δ_i) = Throughfall $_i$ (if calculated for litter layer) or IR $_i$ (if calculated for deeper layers)
2. Net Input$_{layer\ i}$ ($N\Delta_i$) = Δ_i - ET $_{layer\ i}$
3. Soil State$_{layer}$ (SS $_i$) = NΔ_i + Soil Water Content $_{i-1}$
4. Excess of Water$_{layer}$ (EW$_i$) = SS $_i$ - Field Capacity $_{layer\ i}$ (FC $_{layer\ i}$) (When SS$_i$ < FC $_i$, Ew $_i$ = 0)
5. Infiltration Rate$_{layer}$ (IR$_i$) = (parameter that varies with SWC) * (EW $_i$)$^{\wedge 1.8/1000}$
6. Water Balance$_{layer}$ (WB$_i$) = NΔ_i – IR $_i$
7. Final Soil Water Content$_{layer}$ (SWC$_i$) = SWC $_{i-1}$ + NΔ_i – IR $_i$

After the calculations for the first layer, the Net Input$_{layer\ i}$ (NΔ_i) formula for the underlying soil layer changes from Throughfall to the Infiltration Rate (IR$_i$) from the soil layer above, for instance;

Input (NΔ_i _16cm) = IR$_i$ _2cm– ET$_i$_16cm

The final SWC for every soil depth was compared to the actual SWC from the four TDRs installed in every monolith at the same depth, excluding the litter layer. If accurate, the model's IR output could then be compared with the amount of leachate collected by the ZTLs^{3D}. We, however, noticed that following irrigation the WBM yielded slightly retarded increases in soil water content at depth as compared to the TDRs. Hence, also the WBM estimates of drainage fluxes must have been slightly delayed. For this reason, comparisons between the ZTLs and the WBM simulated fluxes were made on cumulative fluxes whenever multiple consecutive collections were available.

3. RESULTS

3.1 Ultrasonic Bath sensitivity analysis

Sensitivity analyses were performed to assure that the material Nylon12 did not interfere with the quality of the sample and make the concentration analyses in the soil leaching the most accurate possible. Figure 5 shows the average of five water samples collected from five pre-washed $ZTLs^{3D}$ (Ultrasonic Bath-UB, Fig. 5) and five non-pre-washed $ZTLs^{3D}$ (No Treatment-NT, Fig. 5). Water was collected from the ZTLs after one, three, six and 30 days, then the water was changed (vertical long-dash line, Fig. 5) and samples were collected again after 45 days since the start of the experiment. Even though results showed a decrease on DOC concentration during the course of the analyses, water samples collected from the pre-washed $ZTLs^{3D}$ (dotted line) always contained lower DOC concentrations than non-pre-washed $ZTLs^{3D}$ (soil-black line).

Even though both sets of $ZTLs^{3D}$ showed a residual DOC concentration at the end of the analysis, that was very small relative to the DOC concentrations typically observed in this study site. Nevertheless, ultrasonic bath pre-treatment showed a lower DOC concentration at any time and is thus recommendable when using nylon $ZTLs^{3D}$ to study DOC leaching.

3.2 Water Bucket Model performance

The WBM reproduced the soil moisture measurements in all treatments very well during the entire study period, from May 2019 till May 2020. Figure 6 and 7 show for all depths and treatments the agreement between modelled data (X-axes) and soil moisture data from TDRs soil sensors (Y-axes). In Figure 6 each data point represented the daily average of four TDRs sensors per monolith and the daily average SWC calculated by the WBM while Figure 7 shows how the model captured the SWC variability perfectly in comparison with the TDRs. The fitted regression lines (blue lines, Fig. 6) were very close to the 1:1 lines (black lines) and R^2 values varied between 0.8 and 0.9 across the different treatments and depths, except for treatment four at 75 cm depth, where a lower R^2 value of 0.71 was obtained.

In the latter case, the low R^2 is related to a disagreement between model and data during heavy rain simulation experiments, when the model likely underestimated infiltration rate, also seen in the bigger modelled SWC compared to the TDRs' SWC (Fig. 7). In addition, the vertical lines seen at low soil moisture levels in some panels in Figure 6 revealed occasional poor model performance when calculating fluctuations at very low soil water contents, also seen in the very low modelled SWC where the WBM did not show as many fluctuations as the TSRs did (Fig. 7). However, this has no impact on $ZTLs^{3D}$ performance because, at these low soil moisture levels, no water drains can be collected.

3.3 Overall (dis)agreement between $ZTLs^{3D}$ and Water Bucket Model

3.3.1 Water collection

Due to the extreme variability in the amount of water collected between sampling dates, depths, and amounts of irrigation, results presented in Figure 8 are separately shown per type of installation (vertical or horizontal), type of rain event (natural or rain simulation) and depths (2, 30 and 75 cm depth) to better visualize the performance of vertically and horizontally installed $ZTLs^{3D}$ through the soil profile. The water volume collected after every natural rain event or rainfall simulation experiment differed between vertical and horizontal types of installation (Fig. 8, panels a vs c and b vs d). However, compared to the amount of leachate water calculated by the WBM, neither installation type worked adequately. For natural rain collections, vertically and horizontally installed ZTLs^{3D} show very similar results at 2 cm depth, while at 30 cm, the vertical installation type collected more water on more frequent occasions. Under natural rains, no collection was possible at 75 cm depth for either installation type. In most cases, both types of ZTLs^{3D} did not collect the volumes of water simulated by the WBM, and often no drainage water was collected at all.

However, following the manipulated rain simulations, a larger number of ZTLs^{3D} collected leaching water. Nevertheless, few ZTLs^{3D} collected similar amounts of modelled leaching water or even overestimated the WBM (markers at or above the 1:1 line in Fig. 8). The best agreement between WBM and ZTLs^{3D} was found with vertically installed ZTLs^{3D} during the irrigation experiments, although even then, R^2 values remained low: $R^2 = 0.33$ at 30 cm depth $R^2 = 0.22$ at 2 cm depth, and $R^2 = 0.18$ at 75 cm depth.

Cumulative collection throughout the entire study period showed the unequal and unpredictable performance of individual ZTLs^{3D}. Figure 9 shows the water collection predicted by the WBM (solid lines) and the actual water collected by all 16 ZTLs^{3D} per depth (dotted/dashed lines) in one specific treatment. This treatment's total surface water input (rain and simulations) was ~8000 ml (recalculated to the same surface area as the ZTLs^{3D}), and total evaporation was estimated at ~570 ml at 2 cm, ~253 ml at 30 cm and ~179 ml at 75 cm. Due to the large soil water deficit at the onset of the measurements, less water drained at deeper depths. Overall, it was evident that none of the ZTLs^{3D} worked consistently, all ZTLs^{3D} underestimated the modelled drainage flow, and huge variation occurred among the ZTLs^{3D} with some hardly ever collecting leachate water (Fig. 9).

3.3.2 Impact of depth

Depth seemed to affect the ZTLs^{3D} performance substantially: the deeper the ZTLs^{3D}, the larger the difference between the volume collected by vertically- or horizontally installed ZTLs^{3D}. Vertically installed ZTLs^{3D} collected more frequently no matter the depth while the performance of horizontally installed ZTLs^{3D} rapidly decreased (Fig. 8 and 9).

Water was sampled most frequently at 2 cm depth while at 30 and 75 cm this was mainly the case after rainfall simulation experiments seen in the filled markers in Figure 8 and in the decrease of cumulative collection through depth in Figure 9. Besides, on 1st February 2019, 3rd June 2019, 1st July 2019, 7th August 2019 and 1st September 2019, collected water volume at 30 cm depth was substantially higher than at 2 cm depth in vertical installation. From September 2019 onwards, the amounts collected decreased with depth. The number of ZTLs^{3D} that collected soil leachate varied in every collection, depending on the amount of rain fallen naturally or simulated but also on the type of ZTLs^{3D} installation and depth (Table 1, Supplementary data).

4. DISCUSSION

4.1 Suitability of Nylon to collect water aimed for DOC analysis

Ultrasonic cleaning has become more popular since it can remove contaminants and clean difficultly accessible areas (Fuchs, 2015). In this research, we performed cleaning of our 3D-printed ZTLs^{3D} to assure that the material used (Nylon12) would not affect the chemical analysis of the collected water. Sensitivity analysis for DOC release showed that ultrasonic baths could avoid sample contamination. We hypothesize that the residue from the samplers' printing process might be released with the first contact with water to do not build up anymore afterwards. This residue would have been captured when sampling with the syringe used to extract samples from the inside of the ZTLs^{3D}, leading to a lower concentration after every sampling as any further measure showed a lower concentration of DOC (Fig. 5) It also leads us to conclude that the material does not reabsorb the possible printing residue as DOC concentration decreases even when new distilled water is added. An even better result might be possible according to Niemczewski (2007), who showed that the cavitation process created in the ultrasonic bath can be stronger at a maximum temperature of 7 ^{o}C while our ultrasonic baths were applied at 60 ^{o}C.

4.2 Water Bucket Model (WBM) validation of drainage water flux

The soil water content simulated with the WBM agreed very well with the TDR measurements in the same plots during the entire study period. However, a lesser agreement was found with extreme soil water contents, especially below 0.05 m^3m^{-3} and when ~75 mm water/day were added in extreme rain simulation experiments. Nevertheless, the lesser agreement for the low SWC did not affect the results of this research as its objective was to compare amounts of water leaching predicted by the model and the actual water leaching collected by the ZTLs^{3D}, which only occurs at higher levels of SWC above FC.

The lesser agreement for the very high SWC is most likely related to the layers' infiltration rates and evapotranspiration. Infiltration rates calculated by the model resulted in a delay of the leachate, mainly at the deepest depths (30 - 75 cm). The bigger the rain simulation, the longer the leachate continues at deeper layers. Kendy *et al.* (2003) found in their water model that soil moisture reacted only after the irrigations for a short period while the soil profile continued draining, generating groundwater recharge throughout the year, resembling our case. The most extreme irrigation events led to underestimated drainage when looking at the results right after the irrigation. According to the WBM, the total drainage at deeper layers was still happening days after the rain simulation, as in reality, the collection with $ZTLs^{3D}$ had already occurred. To account for the infiltration's delay, the total leachate per rain simulation experiment was cumulatively calculated; the same was done in Soldevilla-Martinez et al. (2014): they found that their drainage was more accurate when using cumulative values than daily values. Differently, in natural rain events, the WBM performed excellent and cumulative collections were not needed.

A second explanation for the cause of the infiltration delay in our WBM might be the change of texture through the soil profile. Our WBM does not account for soil properties as texture or organic content, even though every layer has its specific FC and ET. For example, Perreault *et al.* (2013) explained how their model estimates at 30 cm depth were sometimes more accurate than at 5-15cm, which they claim to be due to changes in soil structure in the upper layer (their model uses the same properties for all layers).

4.3 Preferential Flows Pathways, Compaction and "Edge Effect."

Much research is available on specific types of lysimeters, including reviews of different types or comparison of lysimeters with other methods (Abdulkareem *et al.*, 2015), but there is very little research that focuses on the differences between two types of installation of the same Zero Tension Lysimeter. We observed that the amount of water collected depended on the type of installation. Vertically installed $ZTLs^{3D}$ collected larger amounts of water than horizontally installed $ZTLs^{3D}$ throughout the entire study, independent of whether water drainage was caused by natural rain events or by simulations. The difference in the amount of leaching water collected by both installations could be explained by the influence of different types of PFPs (Greve *et al.*, 2010; Hardie *et al.*, 2011) and the effect of compaction created through horizontal installation.

The validation of $ZTLs^{3D}$ with the WBM was considered essential to calculate accurate fluxes of drainage water and DOC leaching and revealed an inconsistent performance of our $ZTLs^{3D}$. According to the WBM, leaching water should have been collected in larger amounts in general for all collections. Several hypotheses described below might explain these discrepancies.

4.3.1 Preferential flow pathways

While collection at 2 cm was always possible, in some cases, at deeper depths (30 cm), we collected larger amounts of water. For example, in 1-February-2019, directly after the initiation of the experiment, the total amount of water collected at 30 cm depth (4883 ml) was more than double that collected at 2 cm depth (1113 ml, Table 1, Supplementary data). These results could be explained by the PFP created by soil coring, as we would expect the column of soil on top of the sampler to be less compact than the rest of the soil. Consequently, water would flow easily through those areas, agreeing with Bergström (1987) who observed that lysimeters with disturbed soil profiles usually had higher drainage volumes than lysimeters with undisturbed profiles.

Collection of higher volumes at 30 cm occurred four times, corresponding to one natural event (June-2019, 3rd Collection) and three irrigation events (1-July-2019, 7-August-2019 and 1-September-2019, Table 1, Supplementary data). Herbaceous plant phenology would have had an impact in the monoliths right after the installation, roots within the monoliths would absorb water after winter, reducing the drainage water from the topsoil, explaining why collection at 30 cm depth was sometimes higher than at 2 cm depth. From September 2019 onwards, the amount of water collected always decreased with depth, independent of the type of event and its intensity. This likely indicates an equilibrium reached by the soil column in texture and its structure few months after the disturbance, representing a recovery of the soil. In the period before, the results of the installations should be treated with care. Recovery times for the soil column during vertical installation was possible since soil was placed back in order of horizons achieving a very similar bulk density and no compaction was produced during installation. Recovery times might change depending on type of soil and climate conditions. In our study, the sandy characteristics of the soil allowed the vertical installation to recover in few months.

4.3.2 Horizontal installation results in soil compaction

Overall, it is clear that horizontal installation created a disturbance that made the sampler not function as it should. It is essential to highlight that pushing the horizontal sampler into the soil column above was considered essential to increase the collection efficiency of ZTLs

(Radulovich & Sollins, 1987). However, it creates soil compaction right above the sampler, forcing the leaching water to avoid the ZTL^{3D} instead of flowing inside. Peters and Durner (2009) indeed highlighted that "the plate lysimeter acts as a barrier for the water flow, so that the pressure head above the lysimeter increases, whereas it decreases underneath the lysimeters”.

The apparent low performance of horizontal installation in this study could thus be explained by the compaction created during installation, as discussed above. In addition, most researchers that used pan lysimeters, which is the most similar sampler to our ZTL^{3D} installed horizontally, use very large pan lysimeters, much wider than our sampler (Makowski *et al.*, 2020; Singh *et al.*, 2018).

These observations follow other studies that concluded that collection efficiency was directly related to bigger collection areas or by reducing water flow around the pan by capillary attraction (Makowski *et al.*, 2020). This confirms why our ZTL^{3D,} with only 8,5 cm width, has a lower efficiency even though, in some cases, pan lysimeters of 250 cm width only achieved a 45% efficiency (Peters and Durner, 2009). Additionally, according to Allaire et al. (2009), pan samplers operate well under wet soil conditions in the presence of macropores. However, they are usually much less efficient in dry soils, which would be the case for our experimental site. Peters and Durner (2009) stated that only in soils with low hydraulic conductivities close to saturation water will be collected regularly, which might explain as well, why ZTLs^{3D} installed horizontally collected much more water during rain simulation events than compared to natural events.

The soil column after horizontal installation did not seem to achieve the same level of recovery than the vertical installation, even after 15 months (time since the installation until the end of the rain simulations), the horizontally-installed ZTLs^{3D} underperformed. We did, however, notice a slight increase in the number of horizontal installed ZTLs^{3D} collecting drainage water during the last rain simulation event (Table 1, Supplementary material during the months of October and November 2019, compared to March 2020). It can therefore not be excluded that waiting much longer following the ZTLs^{3D} installation would have resulted in better efficiency of the horizontally-installed ZTLs^{3D}, but this was not realistic given the limited duration of a PhD study.

4.3.3 The edge effect

The ZTLs^{3D} installed horizontally did not collect as much water as the ones vertically installed. A possible theory that could explain the efficiency difference between vertical and horizontal installation types is "the edge effect", also called “sidewall flow”, generally created during wetting-and-drying cycles (Corwin, 2000). For example, open trenches or isolated monoliths surrounded with plastic foil (as in our study) could lead to an easy preferential flow pathway into a smooth surface, possibly creating lateral flow and, consequently, leaching water avoiding the sampler. For example, in Makowski *et al.* (2020), the volume of water flowing laterally towards the trench equaled 10% of the total irrigated amount in one of their experimental profiles.

4.4 Future outlook

Future development should focus on enhancing the performance of the ZTLs^{3D}, for example by upgrading the sampler structure. We hypothesize that the high water-conductive sand that we placed on top of the ZTLs^{3D} to filter the drainage water may have created a hydrophobic layer that forced the drainage water to bypass the sampler. The same ZTLs^{3D} as described in this paper are currently being used in the Amazon rainforest by the "mamiraura" research group (https://www.mamiraua.org/), and in contrast to our experiment, are performing well. That site is, however, very wet. Due to the climatic conditions, leaching water is more available either by high rainfall or due to the movement of the water table during the flooding months. The high water inputs render the build-up of hydrophobicity unlikely, which may explain why the $ZTLs^{3D}$ are functioning well at this mesic site, whereas they did not perform as expected in the sandy soils of our study site.

The next version of the sampler could therefore replace the high water-conductive sand, prone to become hydrophobic during drought, with a set of 3D printed meshes whose pore size decreases from bigger pores in contact with the soil to smaller pores inside the sampler. This set of meshes could create an easy path for the leaching water into the sampler and avoid the hydrophobicity artifact we speculate is causing most problems.

Once properly functioning, the $ZTLs^{3D}$ could be deployed in whatever ecosystem. However, the $ZTLs^{3D}$ are limited in size and given the heterogeneous nature of water drainage in soils, scaling-up results should be done cautiously, considering the heterogeneity of the soil and adapting the number of $ZTLs^{3D}$ installed to the observed heterogeneity.

As explained above, Nylon 12 is characterized by low moisture absorption (~2%). In the case of using different chemicals in the soil, the $ZTLs^{3D}$ could receive a coating with Dichtol, a chemical safe for food and drinking water, which impregnates the surface of the sampler and minimizes its interactions with the soil and soil water. After printing, Dichtol uses capillarity to infiltrate the material, generating a thin coating. Since any coating could generate hydrophobicity in the sampler structure, we recommend to only coat the inside of the sampler.

5. CONCLUSIONS

Our novel 3D-printed design for Zero Tension Lysimeters allowed collecting leaching water at different depths. Its inert material after an ultrasonic bath allowed accurate chemical analysis. A Water Bucket Model successfully reproduced temporal and spatial variation in soil water content. However, its calculated water fluxes, in general, exceeded the volumes collected by the $ZTLs^{3D}$, indicating that our new $ZTLs^{3D}$ design underestimated the amount of drainage water. Vertically installed $ZTLs^{3D}$ more frequently collected drainage water and typically underestimated drainage water fluxes much less than horizontally installed $ZTLs^{3D}$, independently of the event or depth. This difference could be due to disturbance during installation and soil properties. Preferential flow pathways created by vertical coring would lead to an overestimation as long as the soil has not fully restabilized, whereas compaction and edge effects would underestimate the water flow. Given the potential of the 3D-printed ZTLs, future research should identify the main causes of the low collection efficiency and resolve these artefacts.

Acknowledgements

We would like to thank the Flemish government and the Belgian Science Policy Office (BELSPO) for the financial support of the ForestFlow project number BR/175/A1. We acknowledge Simon Truant from 3DINFINITY for the printing process of the ZTLs^{3D}*. We thank Ignacio Lopez Fenosa for the help when converting the design into a 3D design ready for printing. Special thanks to PhD Lore Verryckt for all the teaching in R coding. We would like to express our gratitude to the group of researchers and technicians of PLECO from UA (Antwerp University) that helped in the very intense field installation of the ZTLs*^{3D} *in the ICOS station of Brasschaat (Belgium), as well as the researchers and technicians from UCL (Université Catholique de Louvain) involved in the field campaign for installation and collection of the ZTLs*^{3D} *in the ICOS station of Vielsalm (Belgium). Finally, we tremendously thank Sunitha Pangala from Lancaster University and Alex Enrich Prast from Linköping University for the outstanding collaboration to install the ZTLs*^{3D} *in the Amazon rain forest (Brasil) as well as for the experience and the knowledge gain.*

Reference list

Abdulkareem, J., Abdulkadir, A. & Abdu, N. 2015. A Review of Different Types of Lysimeter Used in Solute Transport Studies. *International Journal of Plant & Soil Science*, **8**, 1–14, (At: https://doi.org/10.9734/IJPSS/2015/18098. Accessed: 21/3/2022).

Allaire, S.E., Roulier, S. & Cessna, A.J. 2009. Quantifying preferential flow in soils: A review of different techniques. *Journal of Hydrology*, **378**, 179–204, (At: https://doi.org/10.1016/j.jhydrol.2009.08.013. Accessed: 21/3/2022).

Beaman, J.J. & Deckard, C.R. 1990. Selective laser sintering with assisted powder handling, (At: https://patents.google.com/patent/US4938816A/en. Accessed: 21/3/2022).

Bergström, L. 1987. Nitrate Leaching and Drainage from Annual and Perennial Crops in Tile-drained Plots and Lysimeters. *Journal of Environmental Quality*, **16**, 11–18, (At: https://doi.org/10.2134/jeq1987.00472425001600010003x. Accessed: 21/3/2022).

Cabrera Corral, F.J., Bonachela Castaño, S., Fernández Fernández, M.D., Granados García, M.R. & López Hernández, J.C. 2016. Lysimetry methods for monitoring soil solution electrical conductivity and nutrient concentration in greenhouse tomato crops. *Agricultural Water Management*, **178**, 171–179, (At: http://www.sciencedirect.com/science/article/pii/S0378377416303766. Accessed: 21/3/2022).

Corwin, D.L. 2000. Evaluation of a simple lysimeter-design modification to minimize sidewall flow. *Journal of Contaminant Hydrology*, **42**, 35–49, (At: https://doi.org/10.1016/S0169-7722(99)00088-1. Accessed: 21/3/2022).

Dabrowska, D. & Rykala, W. 2021. A Review of Lysimeter Experiments Carried Out on Municipal Landfill Waste. *Toxics*, **9**, 26, (At: https://doi.org/10.3390/toxics9020026. Accessed: 21/3/2022).

Farsad, A., Sadeghpour, A., Hashemi, M., Battaglia, M. & Herbert, S.J. 2019. A review on controlled vacuum lysimeter design for soil water sampling. *Environmental Technology & Innovation*, **14**, 100355, (At: http://www.sciencedirect.com/science/article/pii/S2352186418305029. Accessed: 21/3/2022).

Franz, D., Acosta, M., Altimir, N., Arriga, N., Arrouays, D., Aubinet, M., et al. 2018. Towards long-term standardised carbon and greenhouse gas observations for monitoring Europe´s terrestrial ecosystems: a review. *International Agrophysics*, **32**, 439–455, (At: https://doi.org/10.1515/intag-2017-0039. Accessed: 21/3/2022).

Fuchs, F.J. 2015. 19 - Ultrasonic cleaning and washing of surfaces. In: *Power Ultrasonics* (eds. Gallego-Juárez, J.A. & Graff, K.F.), pp. 577–609. Woodhead Publishing, Oxford, (At: https://doi.org/10.1016/B978-1-78242-028-6.00019-3. Accessed: 21/3/2022).

Gielen, B., Neirynck, J., Luyssaert, S. & Janssens, I.A. 2011. The importance of dissolved organic carbon fluxes for the carbon balance of a temperate Scots pine forest. *Agricultural and Forest Meteorology*, **151**, 270–278, (At: https://doi.org/10.1016/j.agrformet.2010.10.012. Accessed: 21/3/2022).

Greve, A., Andersen, M.S. & Acworth, R.I. 2010. Investigations of soil cracking and preferential flow in a weighing lysimeter filled with cracking clay soil. *Journal of Hydrology*, **393**, 105–113, (At: https://doi.org/10.1016/j.jhydrol.2010.03.007. Accessed: 21/3/2022).

Hardie, M.A., Cotching, W.E., Doyle, R.B., Holz, G., Lisson, S. & Mattern, K. 2011. Effect of antecedent soil moisture on preferential flow in a texture-contrast soil. *Journal of Hydrology*, **398**, 191–201, (At: https://doi.org/10.1016/j.jhydrol.2010.12.008. Accessed: 21/3/2022).

Heiskanen, J., Brümmer, C., Buchmann, N., Calfapietra, C., Chen, H., Gielen, B., et al. 2021. The Integrated Carbon Observation System in Europe. *Bulletin of the American Meteorological Society*, **1**, 1–54, (At: https://doi.org/10.1175/BAMS-D-19-0364.1. Accessed: 21/3/2022).

Horemans, J.A., Janssens, I.A., Gielen, B., Roland, M., Deckmyn, G., Verstraeten, A., et al 2020. Weather, pollution and biotic factors drive net forest - atmosphere exchange of CO2 at different temporal scales in a temperate-zone mixed forest. *Agricultural and Forest Meteorology*, **291**, 108059, (At: https://doi.org/10.1016/j.agrformet.2020.108059. Accessed: 21/3/2022).

IUSS Working Group WRB. 2007. World Reference Base for Soil Resources 2006, first update 2007. World Soil Resources Reports No. 103. FAO, Rome.

Janssens, I.A., Sampson, D.A., Cermak, J., Meiresonne, L., Riguzzi, F., Overloop, S., et al 1999. Above- and belowground phytomass and carbon storage in a Belgian Scots pine stand. *ANNALS OF FOREST SCIENCE*, **56**, 81–90, (At: https://doi.org/10.1051/forest:19990201. Accessed: 21/3/2022).

Kendy, E., Gérard-Marchant, P., Todd Walter, M., Zhang, Y., Liu, C. & Steenhuis, T.S. 2003. A soil-water-balance approach to quantify groundwater recharge from irrigated cropland in the North China Plain: QUANTIFYING RECHARGE IN THE NORTH CHINA PLAIN. *Hydrological Processes*, **17**, 2011–203, (At: https://doi.org/10.1002/hyp.1240. Accessed: 21/3/2022).

Kim, H., Zhao, Y. & Zhao, L. 2016. Process-level modeling and simulation for HP's Multi Jet Fusion 3D printing technology. In: *2016 1st International Workshop on Cyber-Physical Production Systems (CPPS)*, pp. 1–4. IEEE, Vienna, Austria, (At: https://doi: 10.1109/CPPS.2016.7483916. Accessed: 14/06/2022).

Kosugi, K. & Katsuyama, M. 2004. Controlled-Suction Period Lysimeter for Measuring Vertical Water Flux and Convective Chemical Fluxes. *Soil Science Society of America*

Journal, **68**, 371–382, (At: https://doi.org/10.2136/sssaj2004.3710 Accessed: 21/3/2022).

Legout, A., Legout, C., Nys, C. & Dambrine, E. 2009. Preferential flow and slow convective chloride transport through the soil of a forested landscape (Fougères, France). *Geoderma*, **151**, 179–190, (At: https://doi.org/10.1016/j.geoderma.2009.04.002. Accessed: 21/3/2022).

Makowski, V., Julich, S., Feger, K.-H., Breuer, L. & Julich, D. 2020. Leaching of dissolved and particulate phosphorus via preferential flow pathways in a forest soil: An approach using zero-tension lysimeters. *Journal of Plant Nutrition and Soil Science*, **183**, 238–247, (At: https://doi.org/10.1002/jpln.201900216, Accessed: 21/3/2022).

McKeen, L.W. 2017. 8 - Polyamides (Nylons). In: *Film Properties of Plastics and Elastomers (Fourth Edition)* (ed. McKeen, L.W.), pp. 187–227. William Andrew Publishing.

Meissner, R., Rupp, H. & Haselow, L. 2020. *Chapter 7 - Use of lysimeters for monitoring soil water balance parameters and nutrient leaching.* Climate Change and Soil Interactions, Elsevier, pp. 171–205, (At: https://doi.org/10.1016/B978-0-12-818032-7.00007-2. Accessed: 21/3/2022).

Mohamed, R.M.S.R. 2012. Zero-Tension Lysimeter for use in greywater irrigation monitoring. *International Journal of Integrated Engineering*, **4**, (At: https://publisher.uthm.edu.my/ojs/index.php/ijie/article/view/189. Accessed: 21/3/2022).

Neirynck, J., Janssens, I.A., Roskams, P., Quataert, P., Verschelde, P. & Ceulemans, R. 2008. Nitrogen biogeochemistry of a mature Scots pine forest subjected to high nitrogen loads. *Biogeochemistry*, **91**, 201–222, (At: https://www.jstor.org/stable/40343628. Accessed: 21/3/2022).

Niemczewski, B. 2007. Observations of water cavitation intensity under practical ultrasonic cleaning conditions. *Ultrasonics Sonochemistry*, **14**, 13–18, (At: https://doi.org/10.1016/j.ultsonch.2005.11.009. Accessed: 21/3/2022).

Nimmo, J.R. 2012. Preferential flow occurs in unsaturated conditions. *Hydrological Processes*, **26**, 786–789, (At: https://onlinelibrary.wiley.com/doi/abs/10.1002/hyp.8380. Accessed: 22/4/2020).

Perreault, S., Chokmani, K., Nolin, M.C. & Bourgeois, G. 2013. Validation of a Soil Temperature and Moisture Model in Southern Quebec, Canada. *Soil Science Society of America Journal*, **77**, 606–617, (At: https://doi.org/10.2136/sssaj2012.0311. Accessed: 21/3/2022).

Peters, A. & Durner, W. 2009. Large zero-tension plate lysimeters for soil water and solute collection in undisturbed soils. *Hydrology and Earth System Sciences*, **13**, 1671–1683, (At: https://doi.org/10.5194/hess-13-1671-2009. Accessed: 21/3/2022).

Radulovich, R. & Sollins, P. 1987. Improved Performance of Zero-Tension Lysimeters. *Soil Science Society of America Journal*, **51**, 1386–1388, (At: https://doi.org/10.2136/sssaj1987.03615995005100050054x. Accessed: 21/3/2022).

Singh, G., Kaur, G., Williard, K., Schoonover, J. & Kang, J. 2018. Monitoring of Water and Solute Transport in the Vadose Zone: A Review. *Vadose Zone Journal*, **17**, (At: https://doi.org/10.2136/vzj2016.07.0058. Accessed: 21/3/2022).

Soldevilla-Martinez, M., Quemada, M., López-Urrea, R., Muñoz-Carpena, R. & Lizaso, J.I. 2014. Soil water balance: Comparing two simulation models of different levels of complexity with lysimeter observations. *Agricultural Water Management*, **139**, 53–63, (At: https://doi.org/10.1016/j.agwat.2014.03.011. Accessed: 21/3/2022).

Stumpp, C. & Maloszewski, P. 2010. Quantification of preferential flow and flow heterogeneities in an unsaturated soil planted with different crops using the environmental isotope δ18O. *Journal of Hydrology*, **394**, 407–415, (At: https://doi.org/10.1016/j.jhydrol.2010.09.014. Accessed: 21/3/2022).

Thompson, M.L., Scharf, R.L. & Shang, C. 1995. Zero-tension lysimeters: An improved design to monitor colloid-facilitated contaminant transport in the vadose zone. Ames Lab., Ames, IA (United States), (At: https://www.osti.gov/biblio/108103-pd2PVO/webviewable/. Accessed: 7/6/2022).

Veihmeyer, F.J. & Hendrickson, A.H. 1931. The moisture equivalent as measure of the field capacity. *Soil Science*, **32**, 181–194.

Verstraeten, A. 2018. *Evolution of soil solution chemistry in temperate forests under decreasing atmospheric deposition in Flanders*. Dissertation, Ghent University. (At: http://hdl.handle.net/1854/LU-8547603. Accessed: 21/3/2022).

Vogel, T., Gerke, H.H., Zhang, R. & Van Genuchten, M.Th. 2000. Modeling flow and transport in a two-dimensional dual-permeability system with spatially variable hydraulic properties. *Journal of Hydrology*, **238**, 78–89, (At: https://doi.org/10.1016/S0022-1694(00)00327-9. Accessed: 21/3/2022).

Zhu, W., Ock, J., Ma, X., Li, W. & Chen, S. 2015. *Chapter 2 - 3D Printing and Nanomanufacturing*. 3D Bioprinting and Nanotechnology in Tissue Engineering and Regenerative Medicine, pp. 25–55.

Figure legends

Figure 1: Cylindrical ZTL^{3D} design. On the left, "a, b and c" show the external structure of the sampler from three angles, sampler's exits to connect to the extractions tubes are shown in "a", in "b" the external shape from above, rings for easier sampler's extraction are shown in "c". On the right, "d, e and f" are internal parts of the sampler, "d" shows the 10º of inclination at the bottom' sampler, "e" is the printed 1 mm mesh and "f" is the holding ring.

Figure 2: Square ZTL^{3D} design. On the left, "a, b and c" show the external structure of the sampler from three angles, sampler's exits to connect to the extractions tubes are shown in "a", a transparent image in "b" allows to see the internal body sampler and all its components, in "c" the external shape of the sampler from above. On the right, "d, e and f" are the internal parts of the sampler, "d" shows the 10º of inclination at the bottom' sampler, "e" is the printed 1 mm mesh and "f" is the holding ring.

Figure 3: Single plot set up of 14 m^2, four monoliths of 4 m^2 each and how they were isolated from each other.

Figure 4: Three-dimensional representation of the internal disturbance caused to the soil column being measured by one vertical and one horizontal installation in a single monolith (in reality, 12 samplers are installed per 4 m^2 monolith). Red areas represent soil that has been disturbed due to installation and where the ZTL^{3D} may be inserted. Picture made with tinkercad.

Figure 5: DOC concentrations during sensitivity analyses. Ordinates axes indicates the number of days since the start of the analyses when samples were collected. Abscissa axes indicates de concentrations in mgL^{-1} of DOC. Black line represents the average DOC concentrations measured in $ZTLs^{3D}$ that received no treatment after printing (NT). Dotted line represents average DOC concentrations measured in $ZTLs^{3D}$ that received ultrasonic baths before they were filled with distilled water (UB). After 30 days, the emptying and refilling of the $ZTLs^{3D}$ with new distilled water is represented by the vertical long-dash line. Bars on every data point represent Standard Error.

Figure 6: Daily average Soil Water Content (SWC) comparison between the Water Bucket Model (abscissa axes) and TDRs data (ordinate axes). Columns represent treatments while colors represent depths. Blue lines (regression lines) show the agreement with the 1:1 line per depth and treatment.

Figure 7: Time series comparison for the study period. Each panel represents the daily averaged Soil Water Content (SWC) of the soil at four depths. Upper panels show the modelled data by the Water Bucket Model (WBM) while down panels are the SWC provided by the TDRs. Each color corresponds with a specific depth (blue=2cm, orange=30cm, gray=50cm and green=75cm). Every column represent a specific treatment during the study period, which received different rain simulations.

Figure 8: Identity lines comparison from $ZTLs^{3D}$ collections (ordinates axes) versus modelled collections by the WBM (abscissa axes). Natural rain collections are represented by empty markers (ml/ZTL^{3D}). Rain simulation collections are represented by filled markers (ml/ZTL^{3D}). Every data point represents the collection by a single $ZTLs^{3D}$.Circular markers represent vertical installation while square markers represent horizontal installation. Red lines show the agreement with the 1:1 line per depth, type of rain event and type of installation. Each combination has a different name: Vertical installation during Natural collection – "a". Horizontal installation during natural collections –"b". Vertical installation during rain simulations – "c. Horizontal installation during rain simulations – "d". Every row represents a different depth.

Figure 9: Cumulative representation at three depths of the predicted collection in treatment 1 by the WBM (solid lines) compared to the actual collection of 16 vertical (solid colored lines) and horizontally (dashed colored lines) installed $ZTLs^{3D}$ during the study period. Abscissa axes show some of the collection dates.

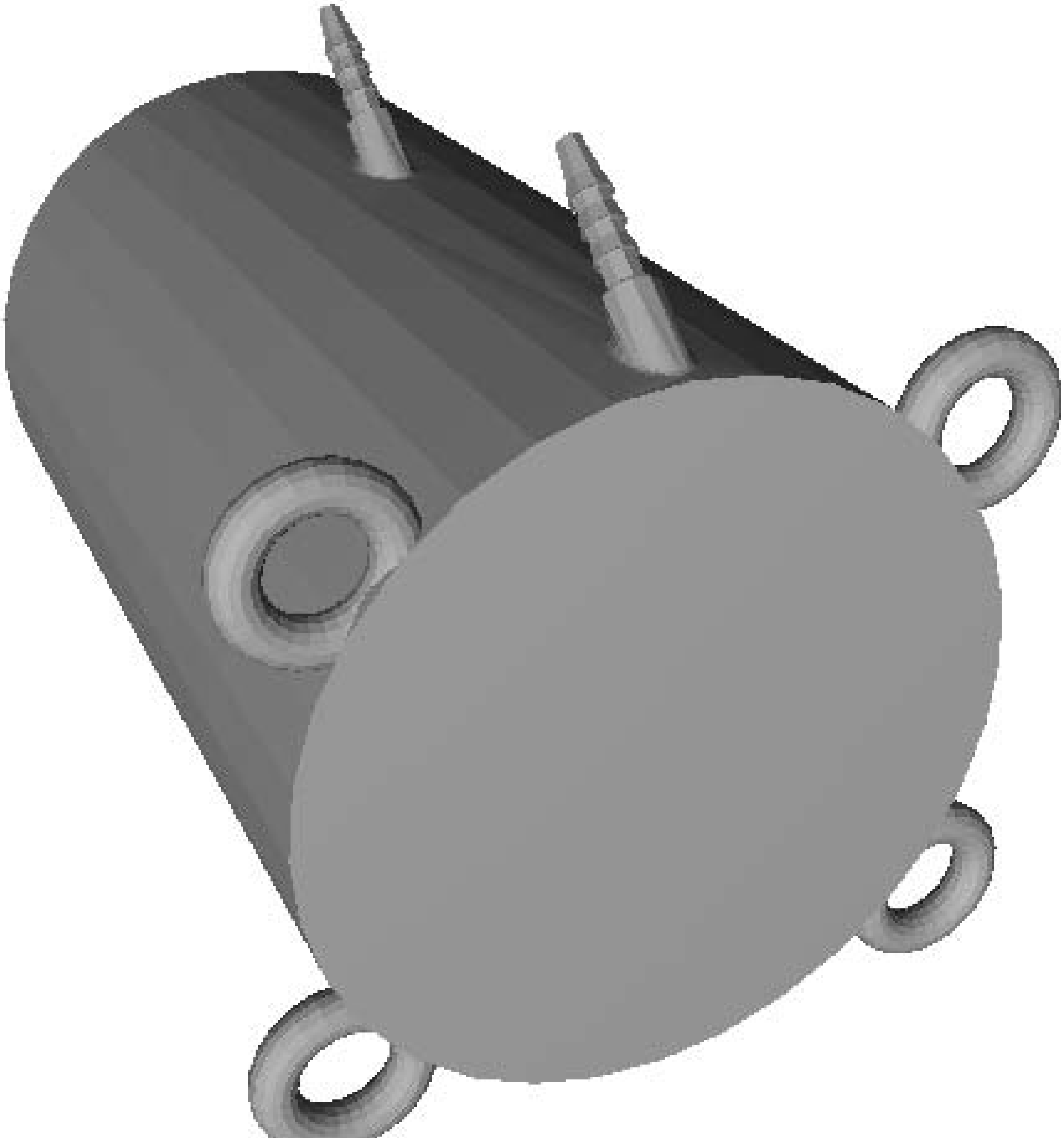

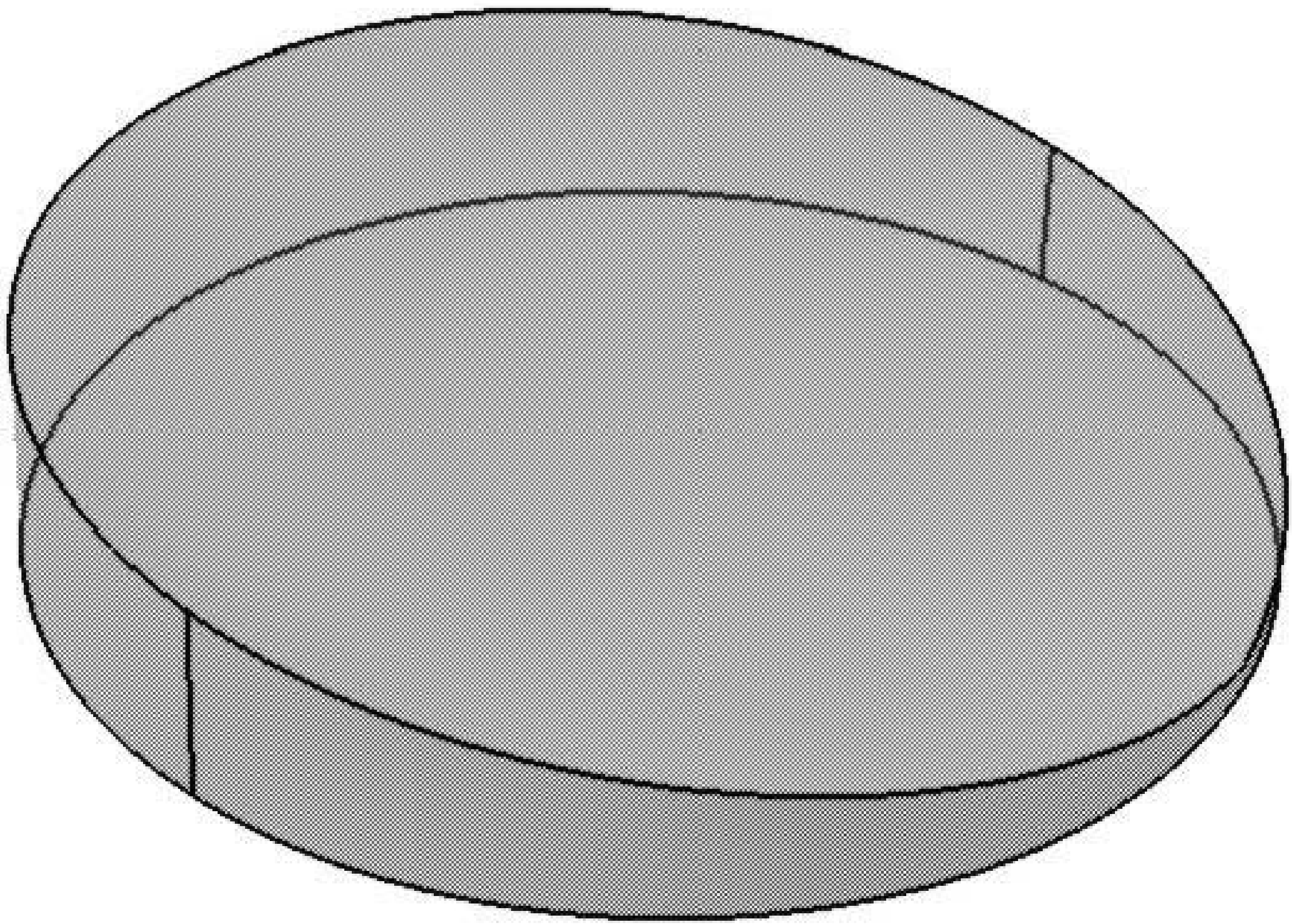

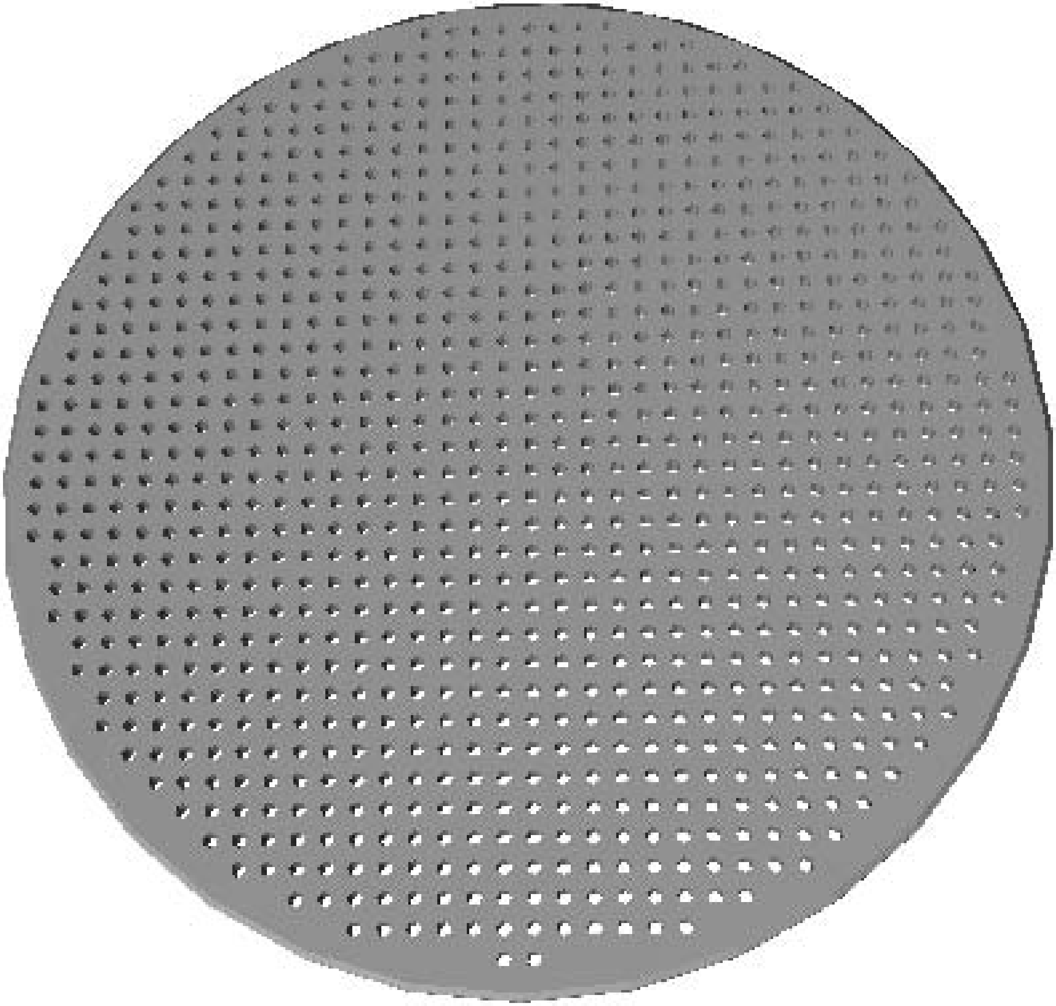

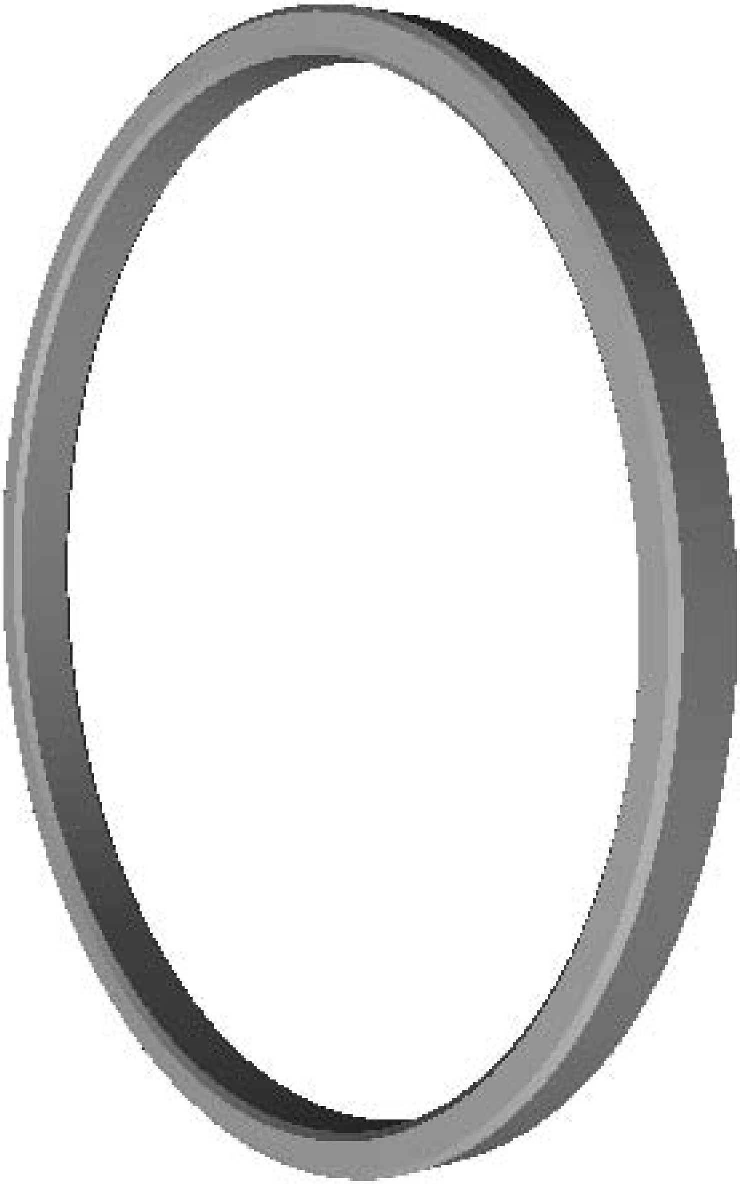

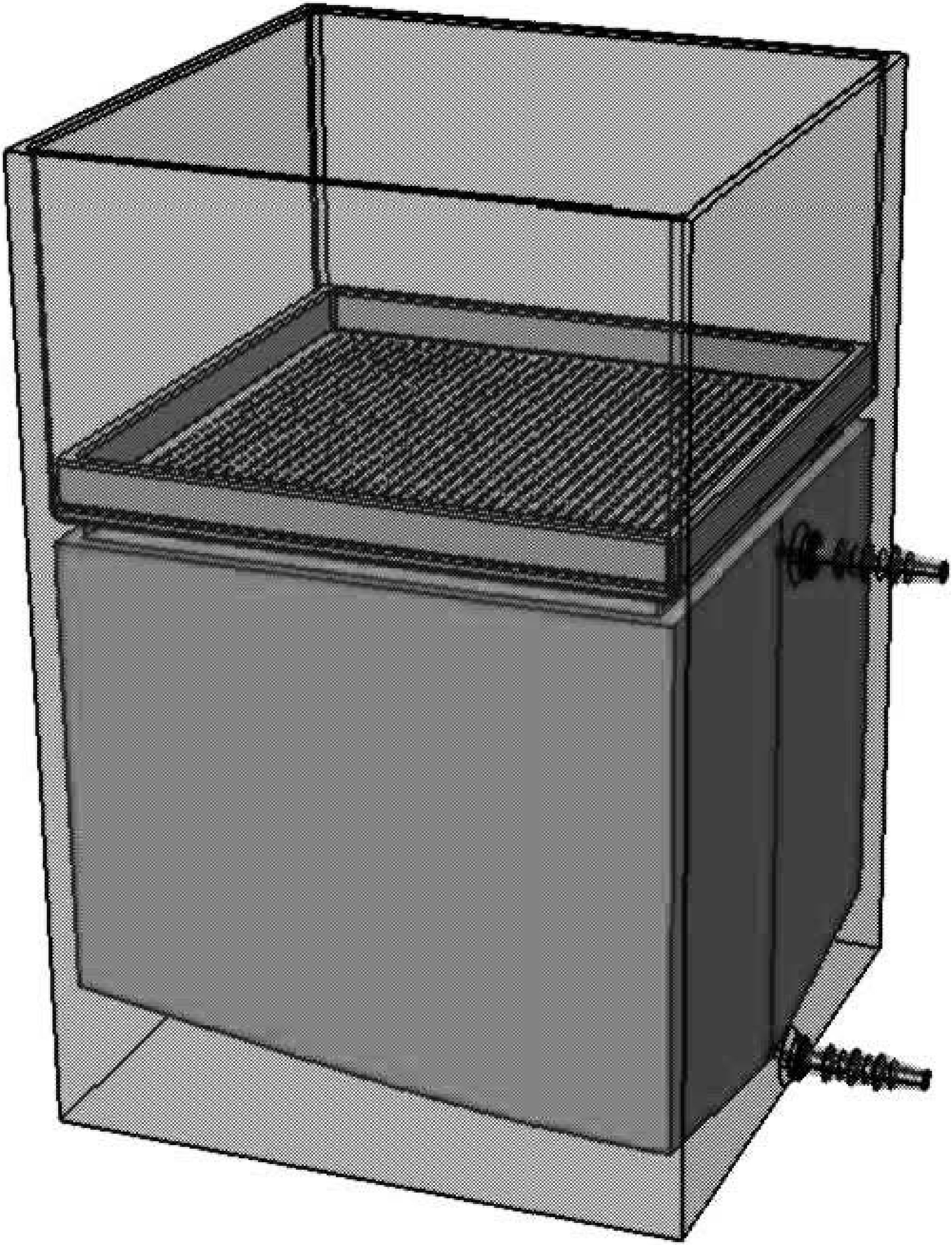

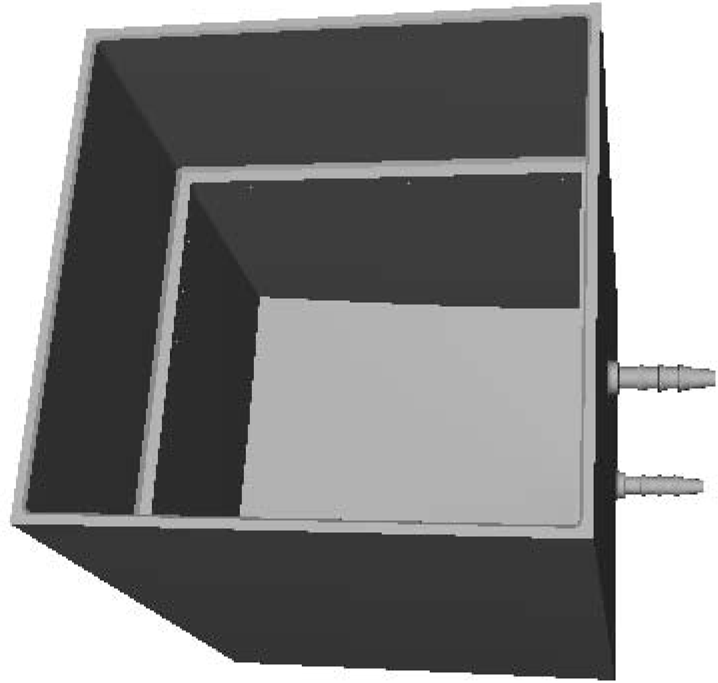

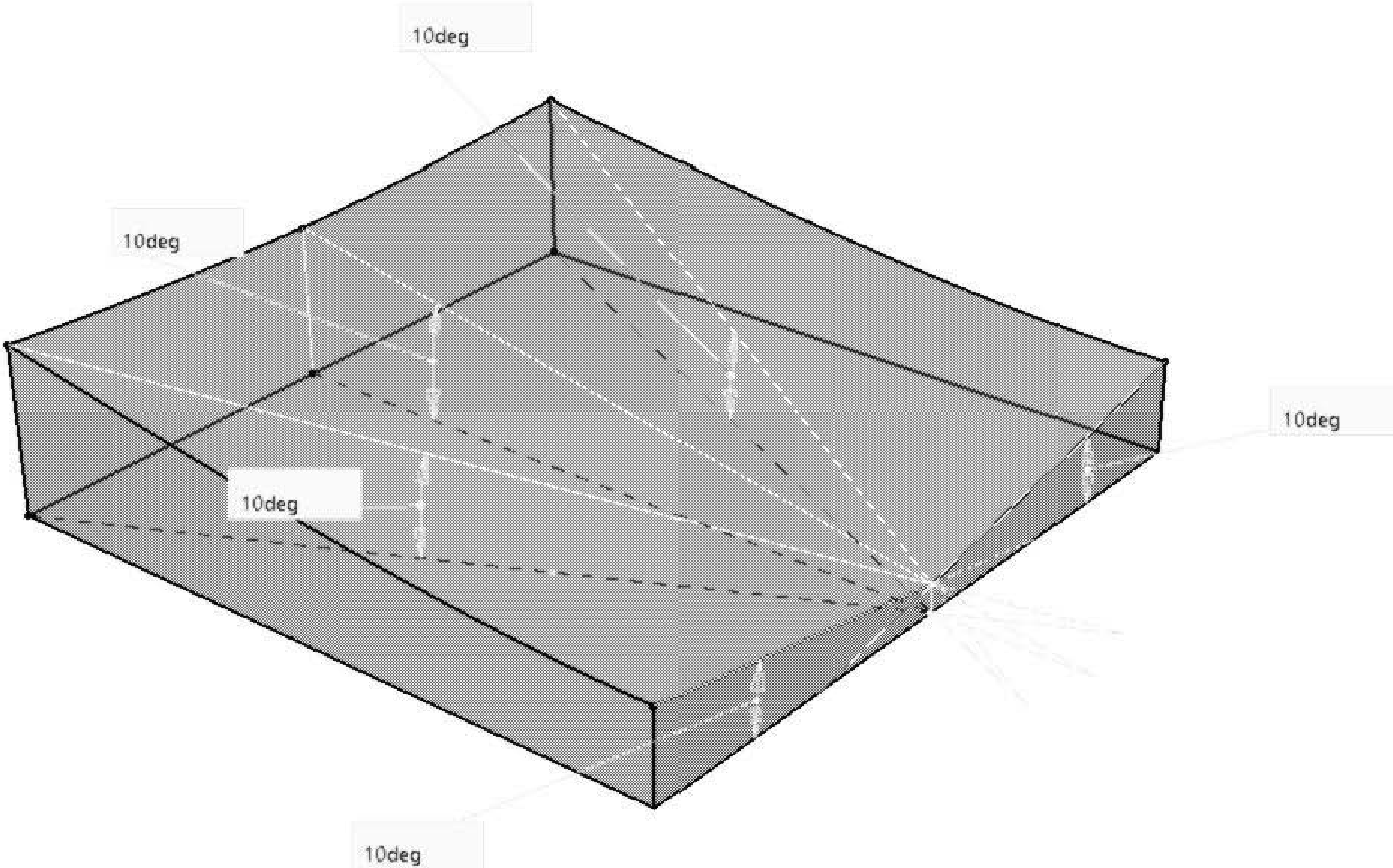
10deg
10deg
10deg
10deg
10deg

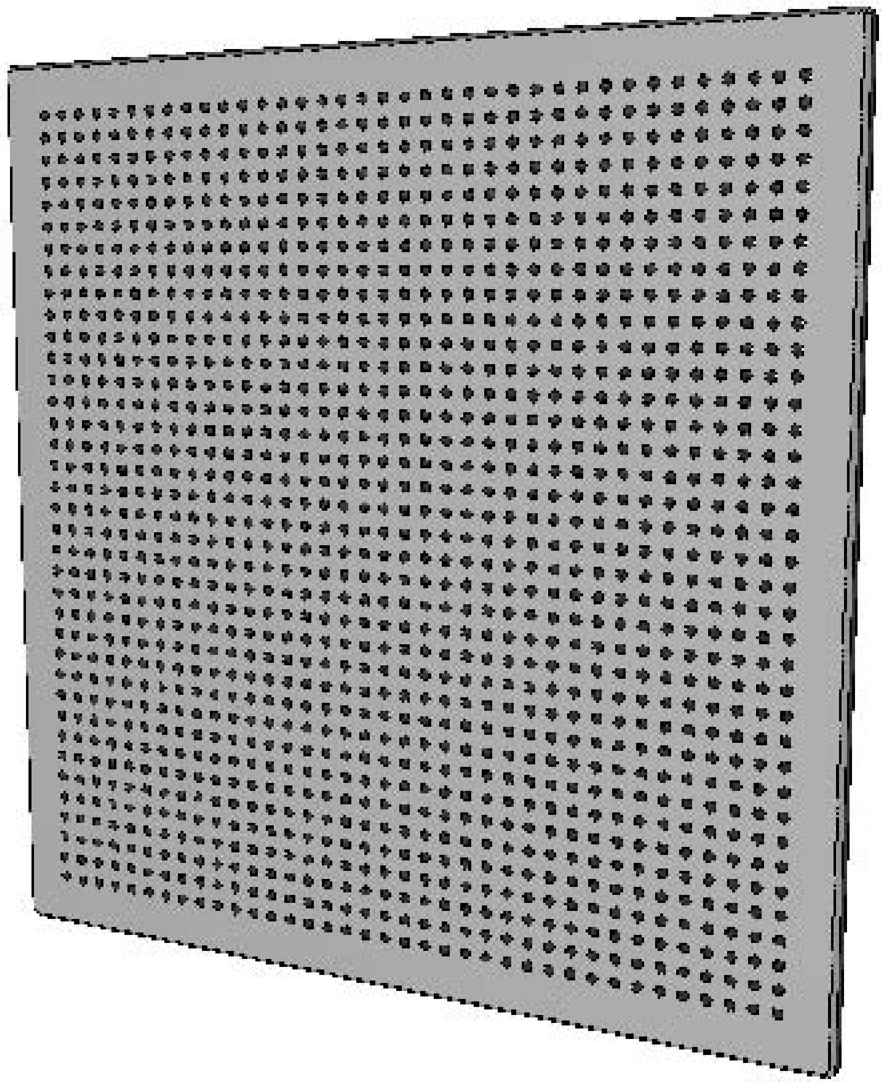

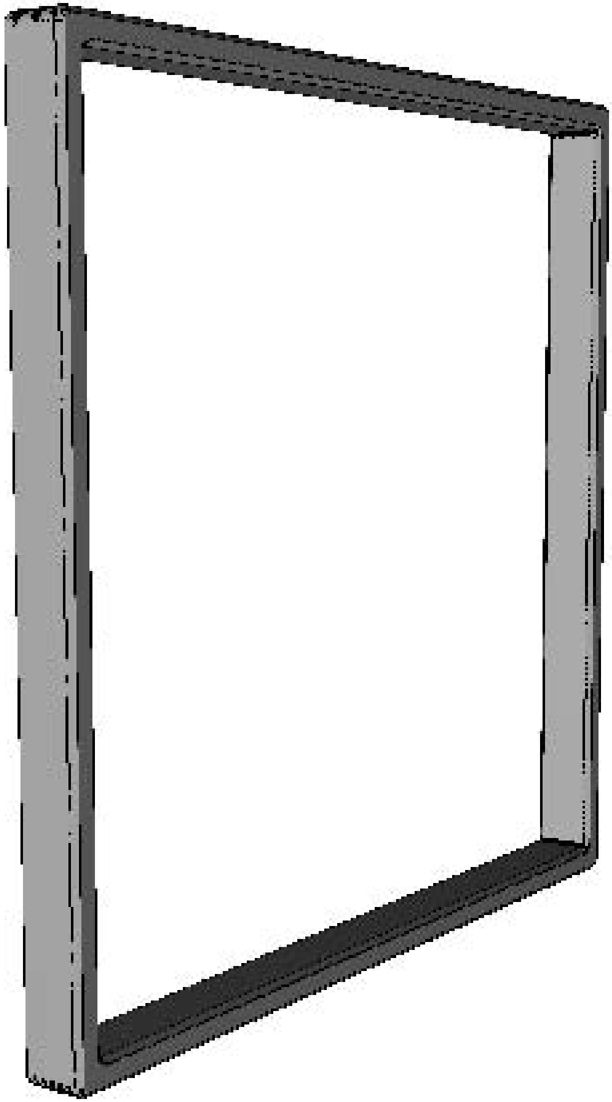

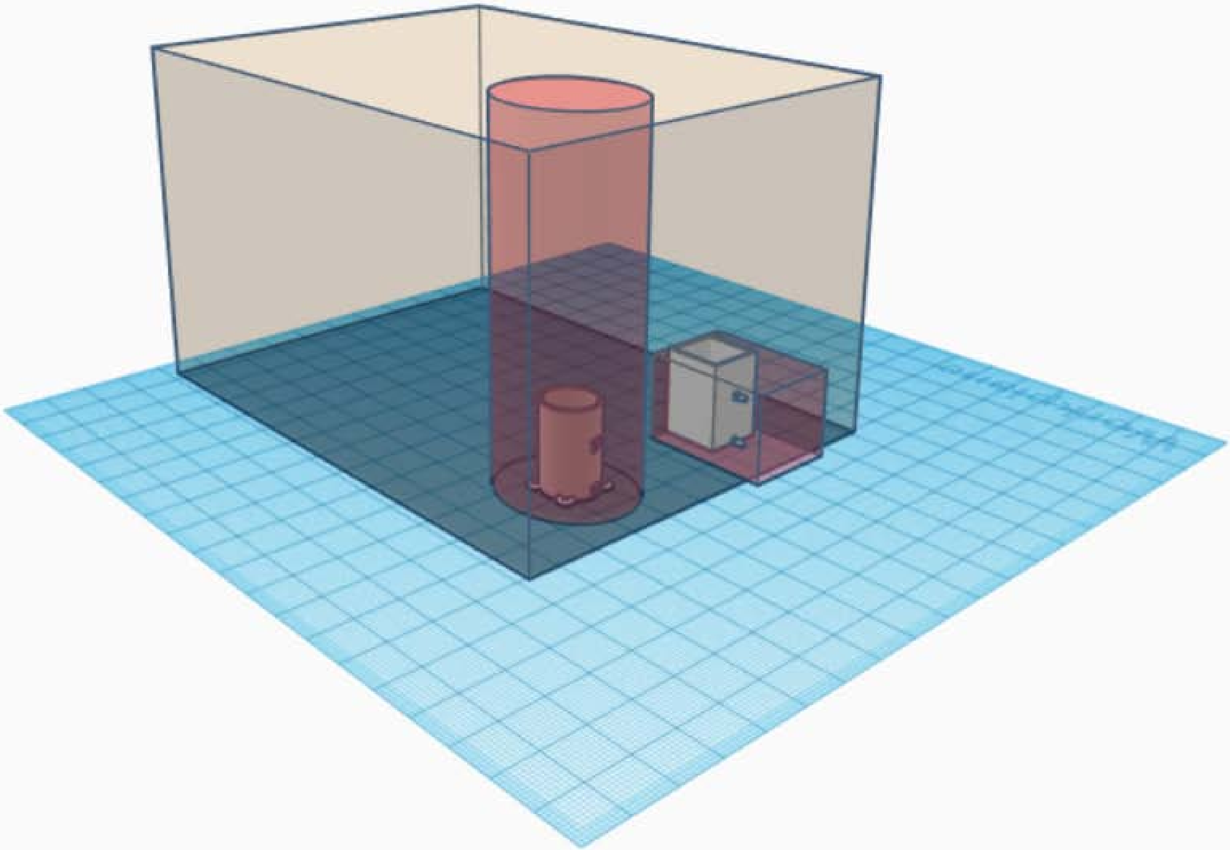

Figure 5

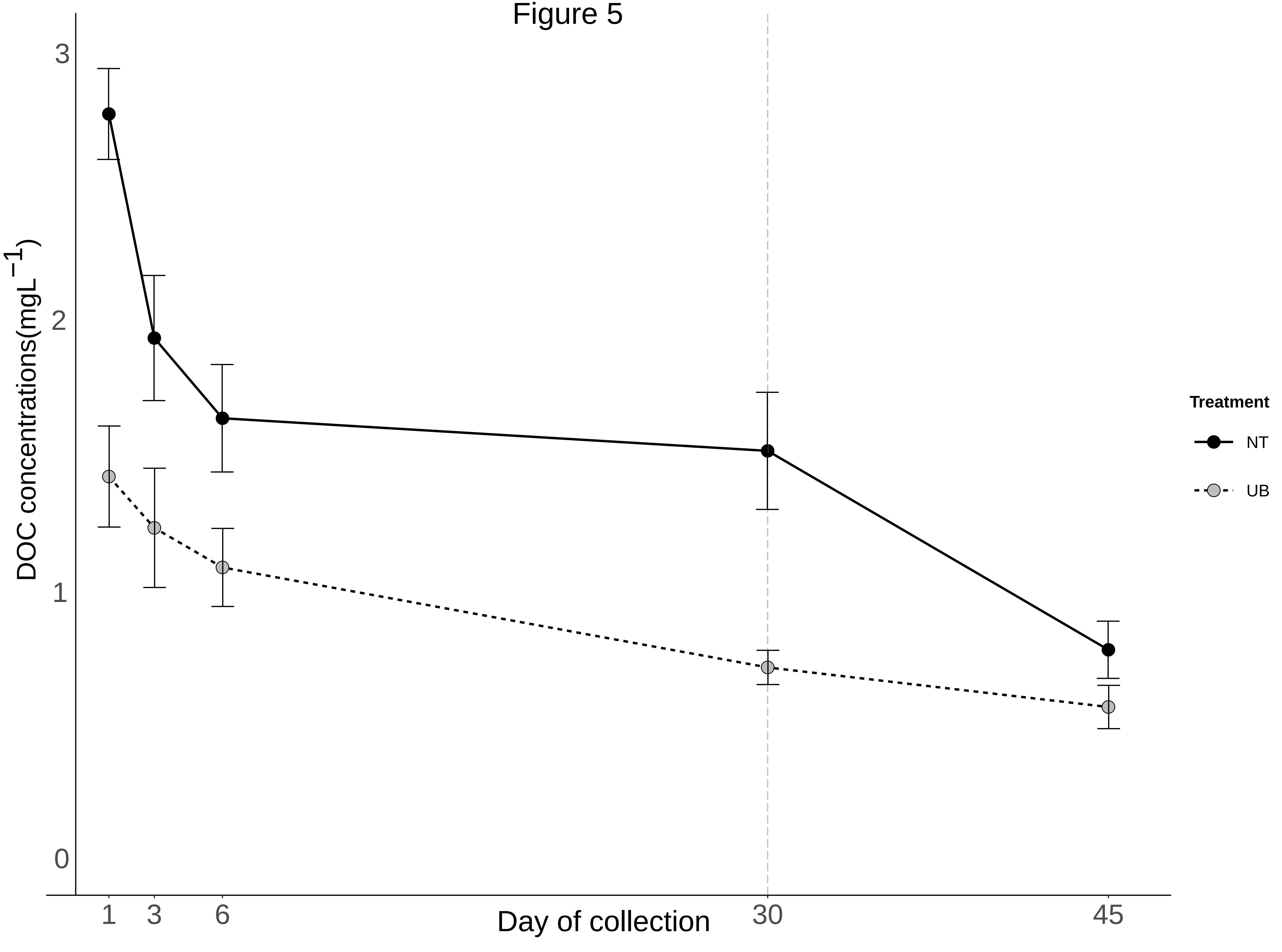

3
2
1
0
DOC concentrations(mgL^{-1})
1
3
6
30
45
Day of collection
Treatment
NT
UB

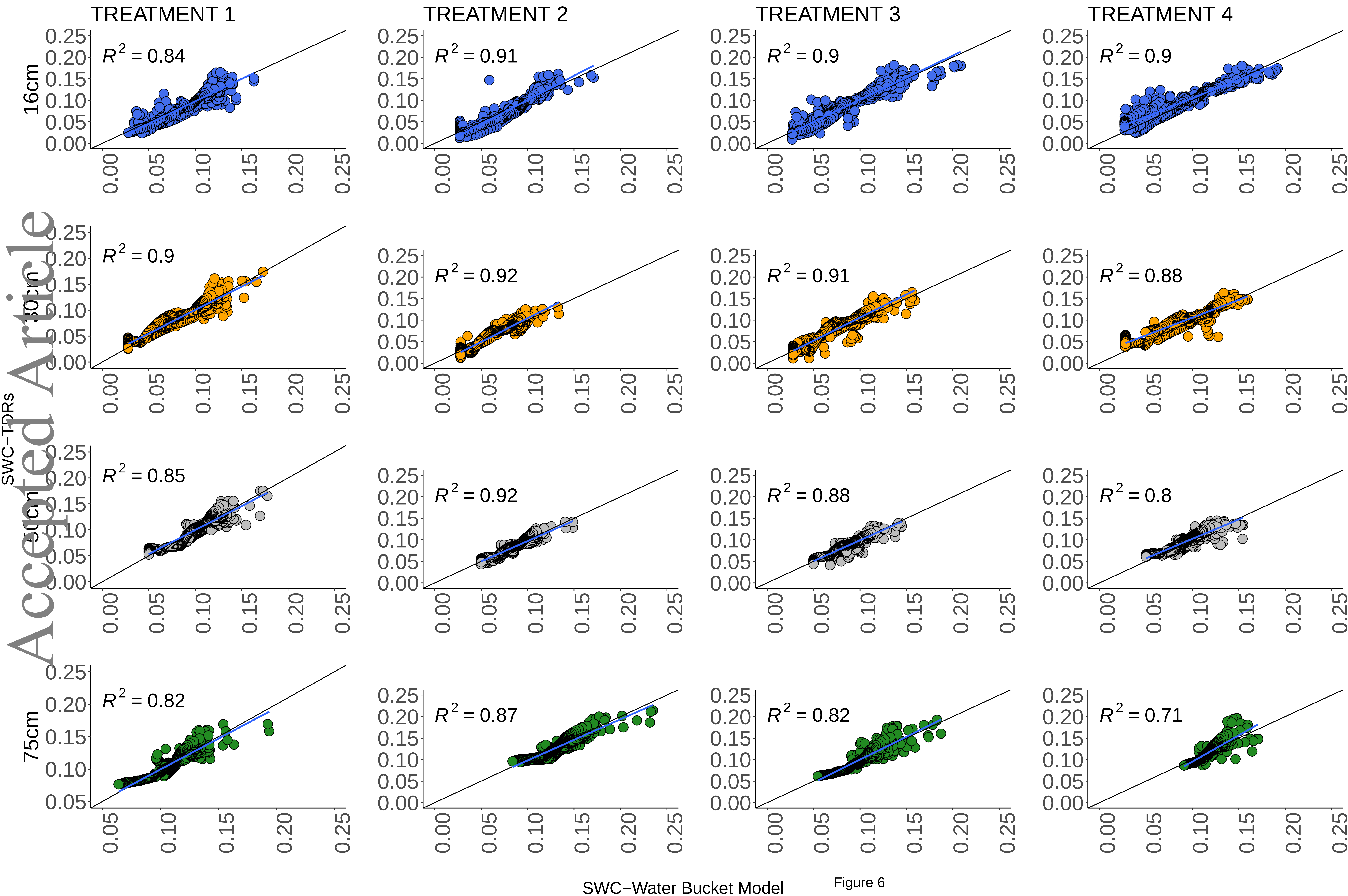
TREATMENT 1
TREATMENT 2
TREATMENT 3
TREATMENT 4
16cm
30cm
50cm
75cm
SWC−TDRs
SWC−Water Bucket Model
$R^2 = 0.84$
$R^2 = 0.91$
$R^2 = 0.9$
$R^2 = 0.9$
$R^2 = 0.9$
$R^2 = 0.92$
$R^2 = 0.91$
$R^2 = 0.88$
$R^2 = 0.85$
$R^2 = 0.92$
$R^2 = 0.88$
$R^2 = 0.8$
$R^2 = 0.82$
$R^2 = 0.87$
$R^2 = 0.82$
$R^2 = 0.71$

Figure 6

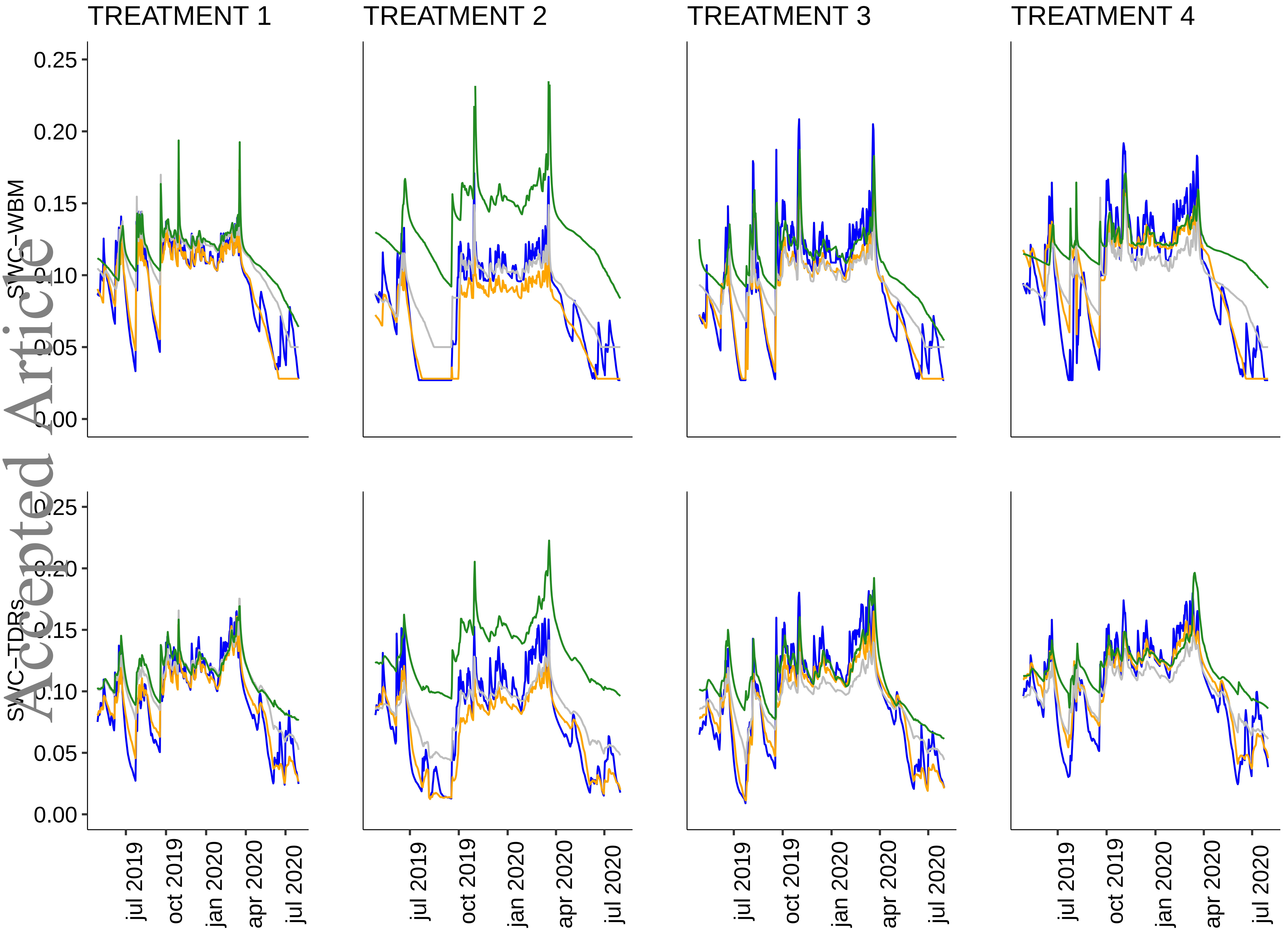
TREATMENT 1
TREATMENT 2
TREATMENT 3
TREATMENT 4
SWC−WBM
SWC−TDRs
0.25
0.20
0.15
0.10
0.05
0.00
jul 2019
oct 2019
jan 2020
apr 2020
jul 2020

Figure 7

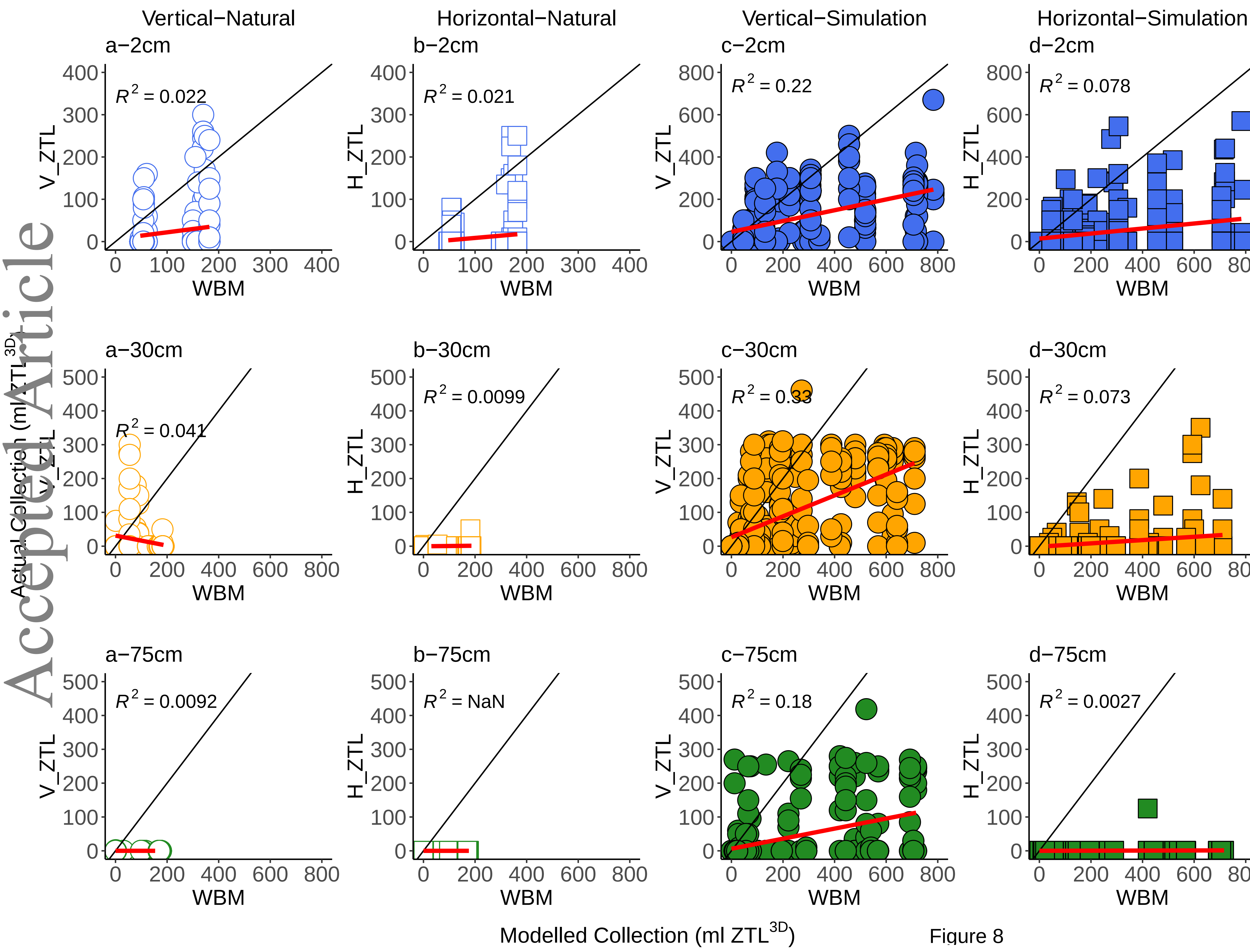
Vertical−Natural
Horizontal−Natural
Vertical−Simulation
Horizontal−Simulation
a−2cm
b−2cm
c−2cm
d−2cm
R^2 = 0.022
R^2 = 0.021
R^2 = 0.22
R^2 = 0.078
a−30cm
b−30cm
c−30cm
d−30cm
R^2 = 0.041
R^2 = 0.0099
R^2 = 0.33
R^2 = 0.073
a−75cm
b−75cm
c−75cm
d−75cm
R^2 = 0.0092
R^2 = NaN
R^2 = 0.18
R^2 = 0.0027
V_ZTL
H_ZTL
WBM
Actual Collection (ml ZTL^{3D})
Modelled Collection (ml ZTL^{3D})

Figure 8

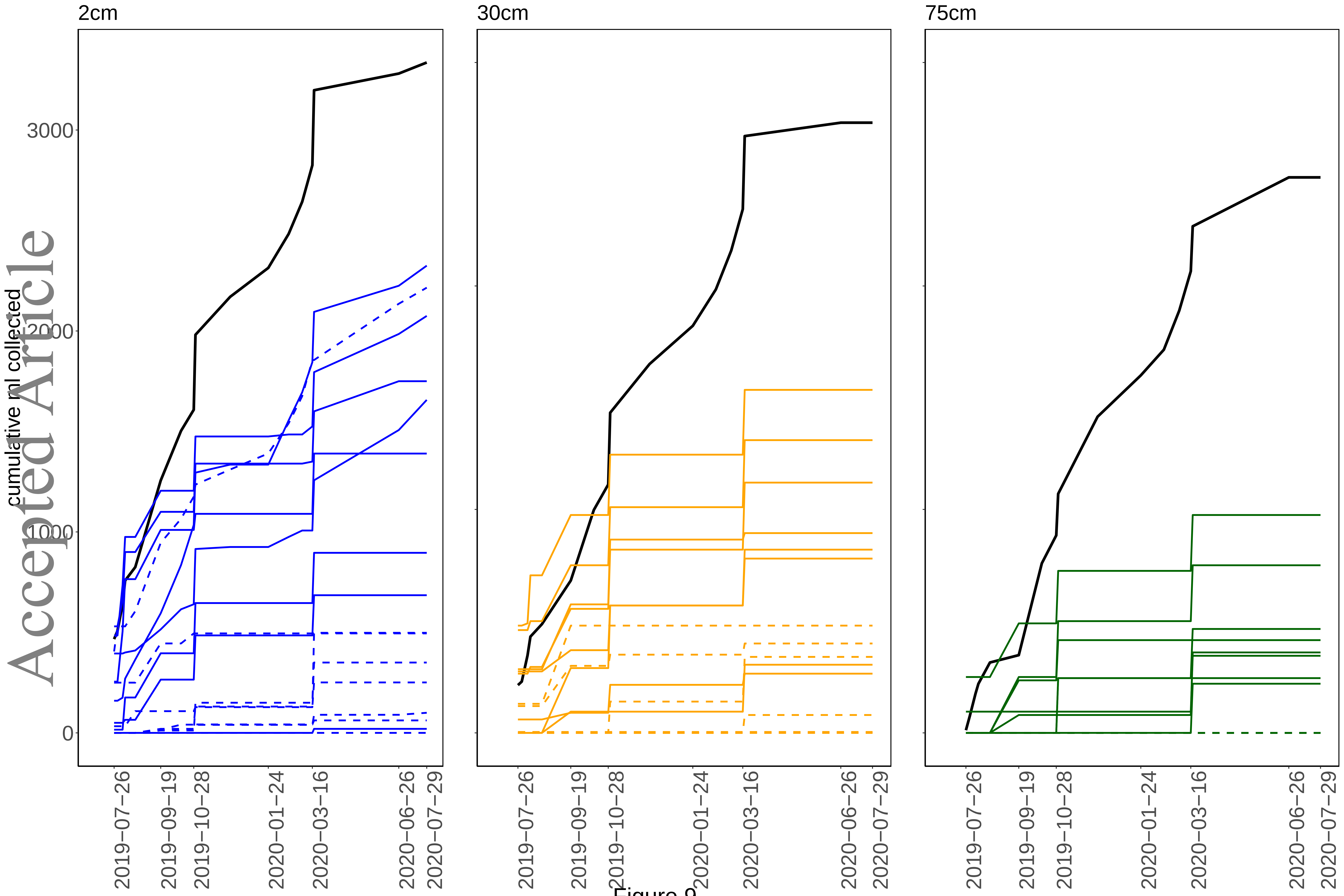
2cm
30cm
75cm
cumulative ml collected
0
1000
2000
3000
2019−07−26
2019−09−19
2019−10−28
2020−01−24
2020−03−16
2020−06−26
2020−07−29

Figure 9